International Journal of Modern Physics E

Viscous Hydrodynamics and the Quark Gluon Plasma

Derek A. Teaney
Department of Physics and Astronomy, Stony Brook University, Stony Brook, New York 11794-3800, United States
derek.teaney@stonybrook.edu

Received (received date)
Revised (revised date)

1. Introduction

One of the most striking observations from the Relativistic Heavy Ion Collider (RHIC) is the very large elliptic flow[48,49]. The primary goal of this report is to explain as succinctly as possible what precisely is observed and how the shear viscosity can be estimated from these observations. The resulting estimates [67,71,72,21,20,57,79,73,70,2] indicate that the shear viscosity to entropy ratio η/s is close to the limits suggested by the uncertainty principle, and the result of $\mathcal{N}=4$ Super Yang Mills theory at strong coupling[65,66]

$$\frac{\eta}{s} = \frac{1}{4\pi}\,.$$

These estimates imply that the heavy ion experiments are probing quantum kinetic processes in this theoretically interesting, but poorly understood regime. Clearly a complete understanding of nucleus-nucleus collisions at high energies is extraordinarily difficult. We will attempt to explain the theoretical basis for these recent claims and the uncertainties in the estimated values of η/s. Further, since the result has raised considerable interest outside of the heavy ion community[76,77], this review will try to make the analysis accessible to a fairly broad theoretical audience.

1.1. *Experimental Overview*

In high energy nucleus-nucleus collisions at RHIC approximately $\sim$ 7000 particles are produced in a single gold-gold event with collision energy, $\sqrt{s} = 200\,\mathrm{GeV/nucleon}$. Each nucleus has 197 nucleons and the two nuclei are initially length contracted a factor of a hundred. The transverse size of the nucleus is $R_{\mathrm{Au}} \sim 5\,\mathrm{fm}$ and the duration of the event is also of order $\sim R_{\mathrm{Au}}/c$. Fig. 1 shows the pre-collision geometry. Also shown is a schematic of the collision vertex and a schematic particle detector

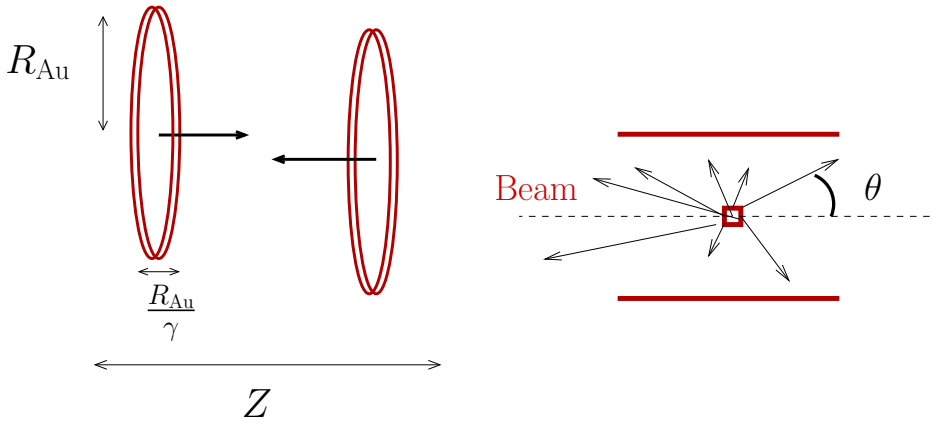

Fig. 1. Overview of a heavy ion event. In the right figure the two nuclei collide along the beam axis usually labeled as Z. At RHIC the nuclei are length contracted by a factor of $\gamma \simeq 100$. The left figure shows the collision vertex of a typical event as viewed in a schematic particle detector and shows a few of the ~ 5000 charged particle tracts recorded per event. The angle θ is usually reported in pseudo-rapidity variables as discussed in the text.

Generically the two nuclei collide off center at impact parameter $\mathbf{b}$ and oriented at an angle Ψ_R with respect to the lab as shown Fig. 2. During the collision the spectator nucleons (see Fig. 2) continue down the beam pipe leaving behind an excited almond shaped region. The impact parameter $\mathbf{b}$ is a transverse vector $\mathbf{b} = (b_x, b_y)$ vector pointing from the center of one nucleus to the center of the other. As discussed in Section 2 both the magnitude and direction of $\mathbf{b}$ can be determined on an event by event basis. We will generally work with the reaction plane coordinates X and Y rather than the lab coordinates.

The elliptic flow is defined as the anisotropy of particle production with respect to the reaction plane

$$v_2 \equiv \left\langle \frac{p_X^2 - p_Y^2}{p_X^2 + p_Y^2} \right\rangle , \tag{1}$$

or the second Fourier coefficient of the azimuthal distribution $\langle \cos(2(\phi - \Psi_R)) \rangle$. Elliptic flow can also be measured as a function of transverse momentum $p_T = \sqrt{p_X^2 + p_Y^2}$ by expanding the differential yield of particles in Fourier series

$$\frac{1}{p_T}\frac{dN}{dy dp_T d\phi} = \frac{1}{2\pi p_T}\frac{dN}{dy dp_T}\left(1 + 2v_2(p_T)\cos 2(\phi - \Psi_{RP}) + \ldots\right) . \tag{2}$$

Here ellipses denote still higher harmonics v_4 and v_6 and so on. In addition the flow can be measured as a function of impact parameter, particle type, and rapidity. For a mid-peripheral collision, $b \simeq 7\,\text{fm}$ the average elliptic flow $\langle v_2 \rangle$ is approximately 7%. This is surprising large. For instance the ratio of particles in the X direction to the Y is $1 + 2v_2 : 1 - 2v_2 \simeq 1.3 : 1$. At higher transverse momentum the elliptic flow grows and at $p_T \sim 1.5\,\text{GeV}$ elliptic flow can be as large as 15%.

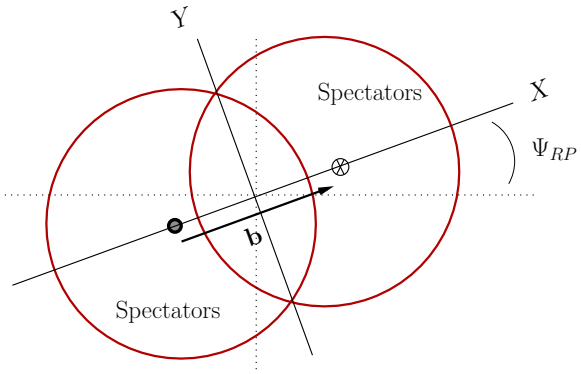

Fig. 2. A schematic of the transverse plane in a heavy ion event. Both the magnitude and direction of the impact parameter **b** can be determined on an event by event basis. X and Y label the reaction plane axes and the dotted lines indicate the lab axis. Ψ_{RP} is known as the reaction plane angle.

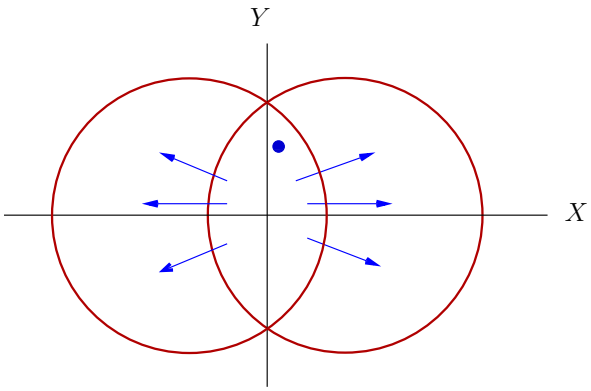

Fig. 3. The conventional explanation for the observed elliptic flow. The spectators continue down the beam pipe leaving behind an excited oval shape which expands preferentially along the short axis of the ellipse. The finally momentum asymmetry in the particle distribution v_2 reflects the response of the excited medium to this geometry. The dot with transverse coordinate $\mathbf{x} = (x, y)$ is illustrated to explain a technical point in Section 2.

1.2. *An interpretation of elliptic flow*

The explanation for the observed flow which is generally accepted is illustrated in Fig. 3. Since the pressure gradient in the X direction is larger than in the Y direction, the nuclear medium expands preferentially along the short axis of the ellipse. Elliptic flow is such a useful observable because it is a rather direct probe of the response of the QCD medium to high energy density created during the event. If the mean free path is large compared to the size interaction region, then the

produced particles will not respond to the initial geometry. On the other hand, if the transverse size of the nucleus is large compared to the interaction length scales involved, hydrodynamics is the appropriate theoretical framework to calculate the response of the medium to the geometry. In a pioneering paper by Ollitrualt the elliptic flow observable was proposed and analyzed based in part on conviction that ideal hydrodynamic models would vastly over-predict the flow [107,108].

However calculations based on ideal hydrodynamics do a fair to reasonable job job in reproducing the observed elliptic flow [51,52,53,54,55]. This has been reviewed elsewhere [3,13]. Nevertheless the hydrodynamic interpretation requires that the relevant mean free paths and relaxation times be small compared to the nuclear sizes and expansion rates. This review will asses the consistency of the hydrodynamic interpretation by categorizing viscous corrections. The principle tool is viscous hydrodynamics which needs to be extended into the relativistic domain in order to address the problems associated with nuclear collisions. This problem has received considerable attention recently and progress has been achieved both at a conceptual [75,8,9,76,69] and practical level [72,79,78,73,74,70]. Generally macroscopic approaches, such viscous hydrodynamics, and microscopic approaches, such kinetic theory, are converging on the implications of the measured elliptic flow [69,1,2,19,21,68]. There has never been an even remotely successful model of the flow with $\eta/s > 0.4$. Since as reviewed in Section 3 η/s is a measure of the relaxation time relative to $\hbar/k_B T$. This estimate of η/s places the kinetics processes measured at RHIC in an interesting and fully quantum regime.

2. Elliptic Flow – Measurements and Definitions

The goal of this section is to review the progress that has been achieved in measuring the elliptic flow. This progress has produced an increasingly self-consistent hydroynamic interpretation of the observed elliptic flow results. This section will also collect the various definitions which are needed to categorize the response the excited medium to the initial geometry.

2.1. *Measurements and Definitions*

As discussed in the introduction (see Fig. 2) both the magnitude and direction of the impact parameter can be determined on an event by event basis. The magnitude of the impact parameter can be determined by selecting events with definite multiplicity for example. For instance, on average the top 10% of events with the highest multiplicity correspond to the 10% events with the smallest impact parameter. Since the cross section is almost purely geometrical in this energy range this top 10% events may be found by a purely geometrical arguement. This line of reasoning gives that the top 10% events with the highest multiplicity are produced by events with impact parameter in the range

$$0 < b < b_* \qquad \text{where} \qquad 10\% = \frac{\pi {b_*}^2}{\sigma_{\rm tot}}\,, \tag{3}$$

where $\sigma_{\rm tot} \simeq \pi(2R_A)^2$ is the total inelastic cross section of the nucleus-nucleus event. After categorizing the top 10% of events we can categorize the top 10-20% of events and so on. The general relation is

$$\left(\frac{b}{2R_A}\right)^2 \simeq \%\ \text{Centrality}\,. \tag{4}$$

Here we have neglected fluctuations and many other effects. For instance there is a small probability that an event with impact parameter $b = 4\,\text{fm}$ will produce the same multiplicity as an event with $b = 0\,\text{fm}$. A full discussion of these and many other issues is given in [32]. The end result is that the impact parameter of a given event can be determined to within say a femptometer.

Given that the impact parameter can be quantified, a useful definition is the number of participating nucleons (also called "wounded" nucleons). The number of nucleons per unit volume in the rest frame of the nucleus is $\rho_A(\mathbf{x}-\mathbf{x}_o, z)$, were $\mathbf{x}-\mathbf{x}_o$ is the transverse displacement from a a nucleus centered at $\mathbf{x}_o$ and z is the longitudinal direction. These distributions are known experimentally and are reasonably modelled by a Woods-Saxon form[32]. The number of nucleons per unit transverse area is

$$T_A(\mathbf{x}-\mathbf{x}_o) = \int_{-\infty}^{\infty} \mathrm{d}z\, \rho_A(\mathbf{x}-\mathbf{x}_o, z)\,, \tag{5}$$

Then, after reexamining Fig. 3, we find that the probability that a nucleon at $\mathbf{x} = (x, y)$ will suffer an inelastic interaction passing through the right nucleus centered $\mathbf{b}/2 = (+\mathrm{b}/2, 0)$ is

$$1 - \exp\left(-\sigma_{\rm NN} T_A(\mathbf{x}-\mathbf{b}/2)\right)\,,$$

where $\sigma_{NN} \simeq 40\,\text{mb}$ is the inelatic nucleon-nucleon cross section at RHIC energies. The number of nucleons which suffer an inelastic collision per unit area is

$$\begin{aligned}\frac{dN_p}{dxdy} &= T_A(\mathbf{x}_\perp + \mathbf{b}/2)\left[1 - \exp\left(-\sigma_{\rm NN} T_A(\mathbf{x}_\perp - \mathbf{b}/2)\right)\right] \\ &\quad + T_A(\mathbf{x}_\perp - \mathbf{b}/2)\left[1 - \exp\left(-\sigma_{\rm NN}\, T_A(\mathbf{x}_\perp + \mathbf{b}/2)\right)\right]\,,\end{aligned} \tag{6}$$

Finally the total number of participants (*i.e.* the the number of nucleons which collide) is

$$N_p = \int \mathrm{d}x\, \mathrm{d}y\, \frac{dN}{dxdy}\,, \tag{7}$$

For a central collision of two gold nuclei the number of participlants $N_p \simeq 340$ is nearly equals the total number nucleons in the two nuclei $N = 394$, leaving about fifty spectators. By comparing the top axis in Fig. 4 to the bottom axis the relationship between participants, impact parameter b, and centrality can be determined.

The reaction plane angle is Ψ_{RP} is also determined experimentally. Here we will describe the Event Plane method which is conceptually the simplest. Assume

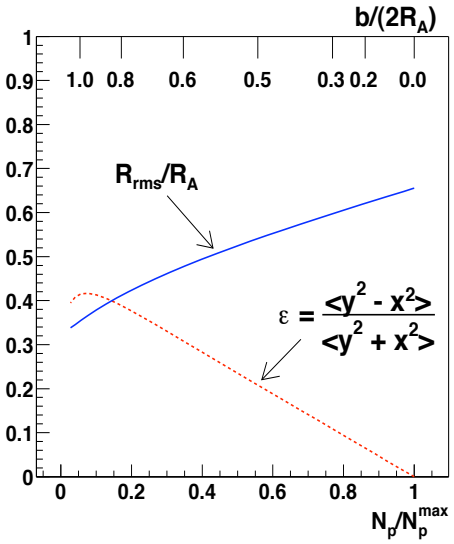

Fig. 4. The eccentricity $\epsilon_{\rm glb}$ as a function of the number of participants relative to the number in a central event $N_p^{\rm max}$. (The number $N_p^{\rm max} \simeq 340$ for a central event.)

frist that the reaction plane angle is known. Then the particle distribution can be expanded in harmonics about the reation plane

$$\frac{dN}{d\phi} \propto 1 + 2v_2 \cos(2(\phi - \Psi_{RP})) + \dots \tag{8}$$

If the number of particles is very large one could simply make a histogram of the angular distribution of particles in an event with respect to the lab axis. Then the reaction plane angle angle would be determined by finding where the histogram is maximum. This is the basis of the event plane method. For all the particles in the event we form the vector

$$\vec{Q} = (Q_x\,, Q_y) = \left(\sum_i \cos 2\phi_i\,,\, \sum_i \sin 2\phi_i \right)\,, \tag{9}$$

Using the continuum appoximation $Q_x \simeq \int \mathrm{d}\phi\, dN/d\phi \cos(2\phi)$ we can estimate the reaction plane angle Ψ_R, from the $\vec{Q}$-vector

$$\frac{\vec{Q}}{|\vec{Q}|} \equiv (\cos(2\Psi_2), \sin(2\Psi_2)) \simeq (\cos(2\Psi_{RP})\,,\, \sin(2\Psi_{RP})) \tag{10}$$

Then we can estimate elliptic flow as $v_2^{\rm obs} \simeq \langle \cos(2(\phi_i - \Psi_2)) \rangle$. The estimated angle Ψ_2 differs from Ψ_{RP} due to statistical fluctuations. Consequently $v_2^{\rm obs}$ will be systematically smaller than v_2 since Ψ_2 is not Ψ_{RP}. This leads to a correction to the estimate given above which is known as the reaction plane resolution. The

final result after considering the dispersion of Ψ_2 relative to the true reaction plane angle Ψ_{RP} is

$$v_2 = \frac{v_2^{\rm obs}}{\mathscr{R}} \qquad \mathscr{R} = \langle \cos 2(\Psi_2 - \Psi_R) \rangle \tag{11}$$

In practice the resolution parameter $\mathscr{R}$ is estimated by dividing a given event into sub-events and looking at the dispersion in Ψ_2 between different sub-events.

There is *a lot* more to the determination of the event plane in practice. Fortunately the various methods has been reviewed recently [38]. An important criterion for the validity of these methods is that the magnitude of elliptic flow be large compared to statistical fluctuations

$$v_2^2 \gg \frac{1}{N} \, . \tag{12}$$

For $v_2 \simeq 7\%$ and $N \simeq 500$ we have $N v_2^2 \simeq 2.5$. Since this number is not particularly large the simple method described above is not completely adequate in practice. The resolution parameter is $\mathscr{R} \simeq 0.7$ in the STAR experiment. At the LHC, estimates suggest that the resolution parameter $\mathscr{R}$ could be as large as $\mathscr{R} \simeq 0.95$. Current methods use 2 particle, 4 particle, and higher cummulants to remove the effects of correlations and fluctuations. These advances are discussed more completely in Section 2.3 and have played an important role in the current estimates of the shear viscosity. The current measurements provide a unique theoretical opportunity to systematically study how hydrodynamics begins to develop in mesoscopic systems.

We now turn several essential trends in the data of elliptic flow. Clearly we would like to measure the response of nuclei to the geomoetry and to this end we categorize the geometry with an assymetry parameter ϵ

$$\epsilon_{\rm s,part} = \frac{\langle y^2 - x^2 \rangle}{\langle y^2 + x^2 \rangle} \, . \tag{13}$$

Traditionally the average $\langle \ldots \rangle$ is taken with respect to the number of participants in the transverse plane, for example

$$\langle y^2 - x^2 \rangle = \frac{1}{N_p} \int {\rm d}x{\rm d}y \, (y^2 - x^2) \frac{dN_p}{dxdy} \, . \tag{14}$$

We will discuss the uncertainty in this number shortly, for the moment we return Fig. 4 which plots the assymmetry parameter versus centrality and also shows the the root mean square radius

$$R_{\rm rms} = \sqrt{\langle x^2 + y^2 \rangle} \, ,$$

which is important for categorizing the size of viscous corrections.

2.2. *Interpretation*

We have collected the essential definitions of ϵ, centrality v_2, and are now in a position to return to the physics. The scaled elliptic flow v_2/ϵ measures the response

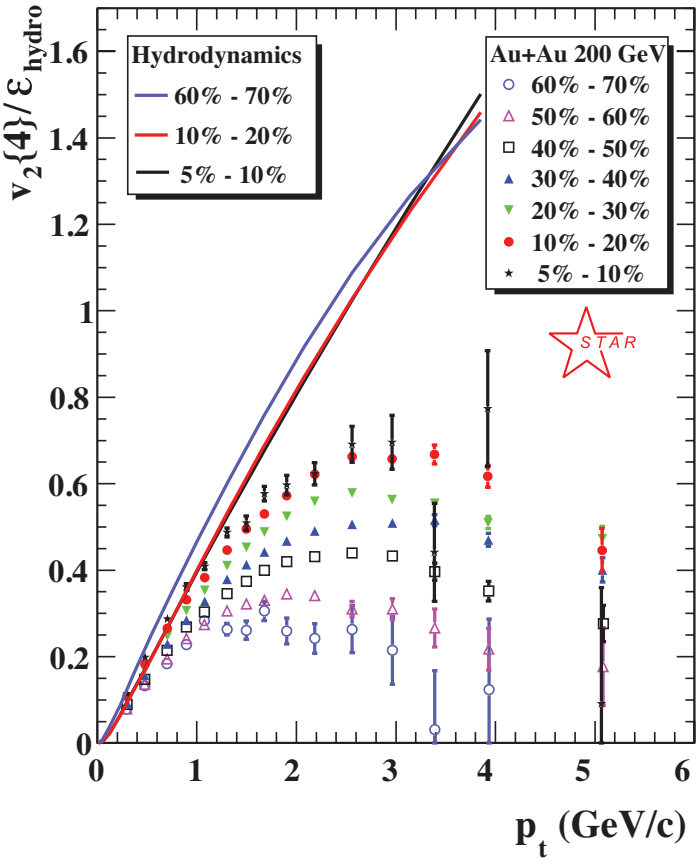

Fig. 5. Elliptic flow as measured by the STAR collaboration[4,5]. The points are shown for different centralities. The measured elliptic flow has been divided by the eccentricity $\epsilon_{\rm hydro}$. The curves are ideal hydrodynamic calculations based upon Refs.[3,54] rather than viscous hydrodynmaics as discussed in much of this work.

of the medium to the initial geometry. Fig. 5 shows $v_2(p_T)/\epsilon$ a function of centrality, 0-5% being the most central and 60-70% being the most peripheral. Examining this figure we see a gradual transition from a weak to a strong dynamic response to the geometry as a funcion of centrality. The interpretation adopted in this review is that this change is a consequence of a system transitioning from a kinetic to hydrodynamic regime.

There are several theoretical curves based upon calculations of ideal hydrodynamics [54,53] which for $p_T < 1\,\mathrm{GeV}$ approximately reproduce the observed elliptic flow in the most central collisions. Since ideal hydrodynamics is scale invariant (for a scale invariant equation of state) the prediction of ideal hydrodynamics is that the response v_2/ϵ should be independent of centrality. This is reasoning is born out by

the more elaborate hydrodynamic calculations shown in the figure. The data on the other hand show a gradual transition as a function of increasing centrality, rising towards the ideal hydrodynamic calcuations in a systematic way. These trends are captured by models a finite mean free path[42].

The data show other trends as a function of centrality. In more central collisions the linearly rising trend, which resembles the ideal hdyrodynamic calculations, extends to larger and larger transverse momentum. We will see in Section 5 that viscous corrections to ideal hydrodynamics grow as

$$\left(\frac{p_T}{T}\right)^2 \frac{\ell_{\rm mfp}}{R}. \tag{15}$$

and this correction restricts the applicable momentum range[71]. Thus in more central collisions, where $\ell_{\rm mfp}/R$ is smaller, the transverse momentum range described by hydrodynamics extends to increasingly large p_T. These qualitative trends are reproduced by the more involved viscous calculations discussed in Section 6.

2.3. *The eccentricity and fluctuations*

Clearly much of the interpretation relies on a solid interpretation of the eccentricity. There are several issues here. First there is the theoretical uncertainty in this average quantity. For example, so far we have defined the "standard glauber participant eccentricity" in Eq. (13). An equally good definition is provided by collision scaling. For instance one measure often used in heavy ion collisions is the number of collisions per transverse area

$$\frac{d^2N_{\rm coll}}{dxdy} = \sigma T_A(\mathbf{x}+\mathbf{b}/2)T_A(\mathbf{x}-\mathbf{b}/2) \tag{16}$$

Then the eccentricity is defined with this weight in the transverse plane. Fig. 6 shows the "standard galuber $N_{\rm coll}$ e ccentricity". Another more sophisticated model is provided by the KLN model which is based on the ideas of gluon saturation [80,40] as implemented in Refs. [113,41]. This model is a safe upper bound on what can be expected for the eccentricity from saturation physics and is also shown in Fig. 6. We can not describe the details of this model and its implementation here. However the physical reason why this model has a sharper eccentricity is the readily understood: the center of one nucleus (nucleus A) passes through the edge of the other nucleus (nucleus B). Since the density of gluons per unit area in the initial wave function is larger in the center of a nucleus relative to the edge, the typical momentum scale of nucleus A ($\sim Q_{s,A}$) is larger nucleus B ($\sim Q_{s,B}$). It is then difficult for the long wavelength (low momentum) gluons in B to liberate the short wavelength gluons in A. The result is that the production of gluons falls off more quickly near the x edge relative to the y edge making the eccentricity larger. Clearly this physics is largely correct although the magnitude of the effect is uncertain. Another estimate based on classical yang mills theory which includes similar physics, but which models the production and non-perturbative sector differently is also shown in Fig. 6 and

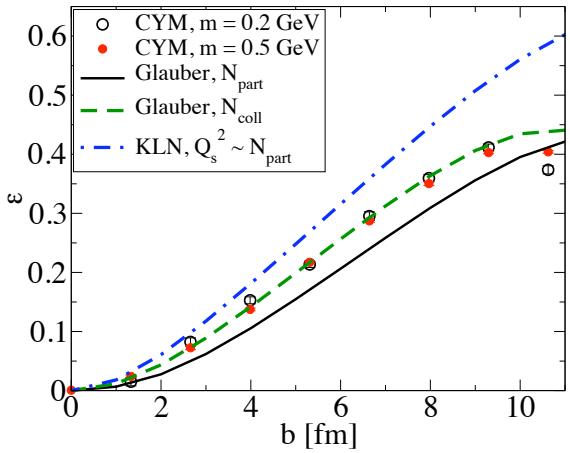

Fig. 6. Figure from Ref.[43] showing various estimates for the initial eccentricity in heavy ion collisons. The physics of the KLN eccentricity is described in the text. The eccentricity is expected to increase with collison energy [42].

finds results similar to $N_{\rm coll}$ scaling [43]. Thus the predictions of the KLN model seem to be a safe upper bound for the eccentricity in heavy ion collisons. Note that an important phenomenological consequence of the the KLN model is that the eccentricity grows with beam energy and is expected to increase about 20% from the RHIC to the LHC [42].

Another important aspect in heavy ion collisions when interpreting the elliptic flow data is fluctuations in the initial eccentricity. These fluctuations are not accounted for in Fig. 6. The history is complicated and is reviewed in Refs.[33,38]. There are fluctuations in the initial eccentricity of the participants especially in periphal AuAu and CuCu collisions. Thus rather than using the continuum approximation given in Eq. (13) it is better to implement a monte carlo glauber calculation and estimate the eccentricity using the "participant plane eccentricity". Fig. 7 illustrates the issue: In a given event the ellipse is tilted and the eccentricity depends on the distibution of participants. This event by event quantity is denoted ϵ_{PP} in the litterature. Clearly the experimental goal is to extract the *response* coefficient C relating the elliptic flow to the eccentricity on an event by event basis

$$v_2 = C\epsilon_{PP}\,. \tag{17}$$

If we assume that the flow methods measure $\langle v_2\rangle$, then we would should simply divide to determine the response, $C = \langle v_2\rangle \,/\, \langle \epsilon_{PP}\rangle$. Making this assumption, the PHOBOS collaboration significantly improved significantly improved the understanding of CuCu data[39]. However, it was generally realized (see in particular.

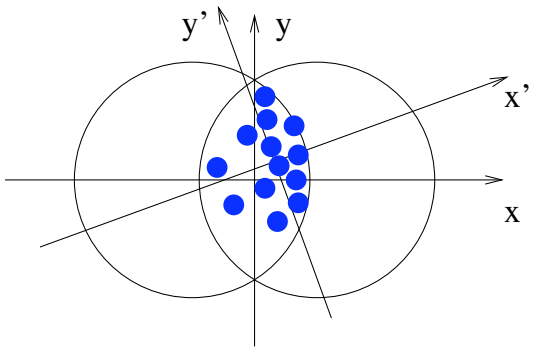

Fig. 7. A figure from Ref.[36] illustrating the participant plane eccentricity ϵ_{PP} in a single event.

Ref.[34]) that the elliptic flow methods measure different things. Some methods methods (such as two particle correlations $v_2\{2\}$) are sensitive to $\sqrt{\langle v_2^2\rangle}$, while other methods (such as the event plane method $v_2\{EP\}$) measure something closer to $\langle v_2\rangle$. What precisely the event plane method measures depends on the reaction plane resolution in a known way[33]. So just dividing by the average participant eccentricity is not entirely correct. The appropriate quantity to divide by depends on the method [34,36,35]. In a gaussian approximation for the eccentricity fluctuations this can be worked out analtyically. For instance, the two paricle correlation elliptic flow $v_2\{2\}$ (which measures $\sqrt{\langle v_2^2\rangle}$), should be divided by $\sqrt{\langle \epsilon_{PP}^2\rangle}$. An important corrolary of this analysis is that $v_2\{4\}$ (v_2 measured from four particle correlations) can be divided by ϵ_s of Eq. (13) to yield a good estimate of the coefficient C. This policy is the one taken in Fig. 5. In the most peripheral AuAu bins and in CuCu the gaussian approximation is poor due to strong correlations amongst the participants[37]. The correlations arise because every participant is assoicated with another participant in the other nucleus. Presumably the last centrality bin in Fig. 5 could be moved up or down down somewhat due to non-gaussian corrections of this sort. With the complete understanding of what each method measures, Ref.[33] was able to make a simple model for the fluctuations and non-flow and show that $\langle v_2\rangle$ measured by the different methods are compatible to an extremely good precision. This work should be extended to the CuCu system where non-gaussian flucutations are stronger and ultimately corroborate the PHOBOS analysisRef.[39,37]. This is a worthwile goal because it will clarify the transition into the hydrodynamic regime [57].

2.4. *Summary*

In this section we have gone into considerable experimental detail – perhaps more than necessary to explain the basic ideas. The reason for this lengthy summary is

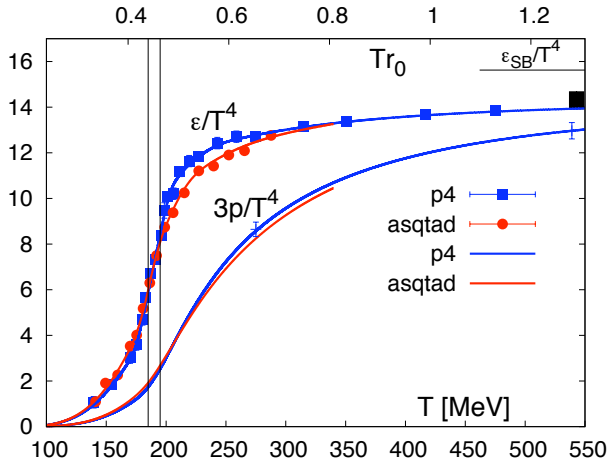

Fig. 8. Figure from Ref.[27] illustrating the energy density and pressure of QCD computed with $N_\tau = 8$ lattice data.

because the trends seen in Fig. 5 were not always so transparent. The relatively coherent hydrodynamic and kinetic interpretation of the observed elliptic flow (which was previewed in Section 2.2 and discussed more completely below) is the result of thoughtful experimental analysis.

3. The Transport coefficients of QCD

In this section we will discuss thermal QCD in equilibrium with the primary goal of collecting various theoretical estimates for the shear viscosity in QCD.

The prominent feature of QCD at finite temperature is the presence of an approximate phase transition from hadrons to quarks and gluons. The equation of state $e(T)$ from lattice QCD calculation is shown in Fig. 8 and shows rapid change for the temperature range $T \simeq 170 - 220\,\mathrm{MeV}$. As estimated in Section 4, the transition region is directly probed during high energy heavy ion collisions.

Well below the phase transition, the gas of hadrons is very dilute and thermodynamics is dominated by the measured particle spectrum. For instance the number of pions in this low temperatures regime is

$$n_\pi = d_\pi \int \frac{\mathrm{d}^3\mathbf{p}}{(2\pi)^3} \frac{1}{e^{E_\mathbf{p}/T} - 1}\,, \tag{18}$$

where $E_\mathbf{p} = \sqrt{p^2 + m_\pi^2}$ and $d_\pi = 3$ accounts for the three fold isospin degeneracy, π^+, π^-, π^0, in the spectrum. If all known particles are included up to a mass $m_{\mathrm{res}} < 2.5\,\mathrm{GeV}$ the resulting Hadron Resonance Gas (HRG) equation of state does a reasonable job of reproducing the thermodynamics up to about $T \simeq 180\,\mathrm{MeV}$. However the validity of this quasi-particle description is unclear above a tempera-

ture of $T \simeq 140, \mathrm{MeV}$ [14]. As the temperature increases, the hadron wave functions overlap until the medium reorganizes into quark and gluon degrees of freedom. Well above the transition the QCD medium evolves to a phase of massless quarks and gluons and the energy density is approximately described by the Stefan-Boltzmann equation of state

$$e_{\rm glue} = d_{\rm glue} \int \frac{\mathrm{d}^3\mathbf{p}}{(2\pi)^3} \frac{E_{\mathbf{p}}}{e^{E_{\mathbf{p}}/T} - 1}\,, \qquad e_{\rm quark} = d_{\rm quark} \int \frac{\mathrm{d}^3\mathbf{p}}{(2\pi)^3} \frac{E_{\mathbf{p}}}{e^{E_{\mathbf{p}}/T} + 1}\,, \tag{19}$$

where $d_{\rm glue} = {}_{2\times8}$ counts spin and color, and $d_{\rm quark} = {}_{2\times2\times3\times3}$ counts spin, anti-quarks, flavor, and color. Performing these integrals we find $e_{SB} = e_{\rm glue} + e_{\rm quark} \simeq 15.6\, T^4$ as illustrated by the line in the top-right corner of the figure.

We have described the particle content well above and well below the transition. Near the approximate phase transition the validity of such a simple quasi-particle description is not clear. The transition is a rapid cross-over where hadron degrees of freedom evolve into quark and gluon degrees of freedom rather than a true phase transition. All correlators change smoothly, but rapidly, in a temperature range of $T \simeq 170 - 210$. From a phenomenological perspective the smoothness of the transition suggests that the change from quarks to hadrons should be thought of a soft process rather than an abrupt change.

To address whether the heavy ion reactions produce enough material, over a large enough space-time volume to be described in thermodynamic terms, the relevant medium property is not the equation of state but the transport coefficients. The shear and bulk viscosities govern the transport of energy and momentum and are clearly the most important.

In Section 4 and Section 5 we will describe the role of shear viscosity in the reaction dynamics. The purpose here is to summarize the results of various computations of shear viscosity. A good way to implement this summary is to form shear viscosity to entropy ratio, η/s [66]. To motivate this ratio we remark that it seems difficult to transport energy faster than a quantum time scale set by the inverse temperature,

$$\tau_{\rm quant} \sim \frac{\hbar}{k_B T}\,.$$

A sound wave propagating with speed c_s will diffuse (spread out) due to the shear viscosity. Linearized hydrodynamics shows that this process is controlled by the momentum diffusion coefficient $D_\eta = \eta/(e+p)$ (see for example [115].) Noting the diffusion coefficient has units of (distance)^2/time, a kinetic theory estimate for the diffusion process yields

$$\frac{\eta}{e+p} \sim v_{\rm th}^2 \tau_R\,, \tag{20}$$

where τ_R is the particle relaxation time and $v_{\rm th}^2 \sim c_s^2$ is the particle velocity. Dividing by the $v_{\rm th}^2$ and using the thermodynamic estimates

$$sT \sim e v_{\rm th}^2 \sim p \sim n\, k_B T\,, \tag{21}$$

we see that

$$\frac{\eta}{s} \sim \tau_R T \sim \frac{\hbar}{k_B}\frac{\tau_R}{\tau_{\rm quant}}\,, \tag{22}$$

Thus η/s is the ratio between the medium relaxation time and the quantum time scale $\tau_{\rm quant}$ in units of $\hbar/k_B$, *i.e.* a measure of the transport time in "natural untis".

In the dilute regime the ratio between the medium relaxation time and the quantum time scale is long and kinetic theory can be used to calculate the shear viscosity to entropy ratio. First we consider a simple classical massless gas with particle density n and a constant hard sphere cross section σ_o. The equation of state of this gas is $e = 3p = 3nT$ and the shear viscosity is computed using kinetic theory

$$\eta \simeq 1.2\frac{T}{\sigma_o} \tag{23}$$

The entropy is $s = (e+p)/T$ and the shear to entropy ratio is

$$\frac{\eta}{s} \simeq 0.3\,\frac{T}{n\sigma_o} \tag{24}$$

In what follows, this calculation will provide a qualitative understanding of more sophisticated kinetic calculations.

In the dilute hadronic regime, η/s was calculated in Ref.[100] using measured elastic cross sections for gas of pions and kaons. In the $\pi\pi$ phase shifts there is a prominent ρ resonance, while in the πK channel there is a prominent K^* resonance. Thus the equation of state of this gas is well modeled by an ideal gas of π, K, ρ and K^* [30,31]. The viscosity of this mixture was computed in Ref.[100] and the current author digitized this viscosity, computed the entropy, and determined the η/s ratio. This is shown in Fig. 9. Similar though slightly larger values were obtained in Ref.[14] which also estimated the range of validity for hadronic kinetic theory, $T \lesssim 140\,\mathrm{MeV}$. Finally a more involved Kubo analysis of the UrQMD hadronic transport model [26] (which includes many resonances) is also displayed in Fig. 9.

At asymptotically high temperatures the coupling constant α_s is weak and the shear viscosity can be computed using perturbation theory. Initially, only $2 \to 2$ elastic scattering was considered, and the shear viscosity was computed in a leading log plasma with self consistent screening [64]. Later it was recognized [28,29] that that collinear Bremsstrahlung processes are important for the calculation of shear viscosity and this realization ultimately resulted in a complete leading order calculation [63]. We can estimate η/s in the perturbative plasma using Eq. (23) with $s \propto T^3$ and $\sigma \propto \alpha_s^2/T^2$,

$$\frac{\eta}{s} \sim \frac{1}{\alpha_s^2}\,. \tag{25}$$

The final result from a complete calculation is reproduced in Fig. 9. There are many scales in the problem and it is difficult to know what precisely to take for the Debye

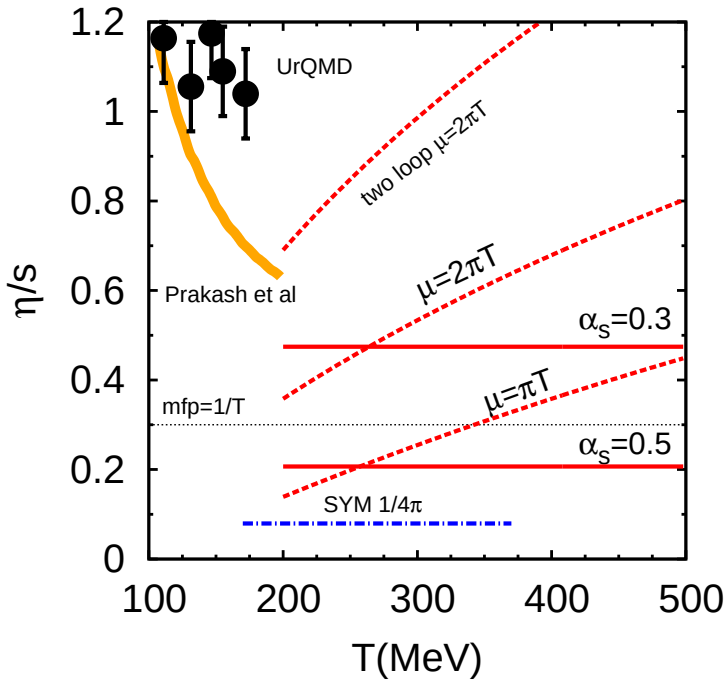

Fig. 9. (Color Online) A compilation of values of η/s. The results from Prakash *et al* are from Ref.[100] and describe a meson gas of pions and kaons (and indirectly K^* and ρ) computed with measured cross sections. The black points are based on a Kubo analysis of the UrQMD code which includes many higher resonances [26]. The red lines are different implementations of the AMY (Arnold, Moore, Yaffe) calculation of shear viscosity [63]. In each curve the Debye scale is fixed $m_D = 2T$. In the dashed red curves the (one loop three flavor) running coupling is taken at the scale μ. In the solid red curves α_s is kept fixed. The two loop running coupling is shown with $\mu = 2\pi T$ for comparison. In the AMY curves, changing the Debye mass by $\pm 0.5T$ changes η/s by $\sim \pm 30\%$. Finally the thin dashed line indicates a simple model discussed in the text with $\ell_{\rm mfp} = 1/T$.

mass and the coupling constant. At lowest order in the coupling the Debye mass is[25]

$$m_D^2 = \left(\frac{N_c}{3} + \frac{N_f}{6}\right) g^2 T^2 \,, \tag{26}$$

which is too large to be considered reliable. For definiteness we have evaluated the leading coupling constant at a scale of πT and set the Debye mass to $m_D = 2T$. The resulting value of η/s is shown in Fig. 9. Various other alternatives are explored in the figure and underscore the ambiguity in these numbers.

Clearly all of the calculations presented have a great deal of uncertainty around the phase transition region. On the hadronic side there are a large number of inelastic reactions which become important On the quark gluon plasma side, the strong dependence on the Debye scale and the coupling constant is disconcerting. It is

very useful to have a strongly coupled theory where the shear viscosity to entropy ratio can be computed exactly. In strongly coupled $\mathcal{N} = 4$ Super Yang Mills theory with a large number of colors η/s can be computed using gauge gravity duality and yields the result [65,66]

$$\frac{\eta}{s} = \frac{1}{4\pi}\,. \tag{27}$$

From the perspective of heavy ion physics this result was important because it showed that there exist field theories where η/s can be this low. Although $\mathcal{N} = 4$ has no particle interpretation, we note that extrapolating Eq. (23) by setting $\ell_{\rm mfp} = 1/n\sigma_o = 1/\pi T$ yields a value for η/s which is approximately equal to the SYM result. In Fig. 9 we have displayed this numerology with $\ell_{\rm mfp} = 1/T$ for clarity.

There are many aspects of transport coefficients which have not been reviewed here. For instance, there is an ongoing effort to determine the transport coefficients of QCD from the lattice [12,11]. While the precise determination of the transport coefficients is very difficult [61,116,115], the lattice may be able to determine enough about the spectral densities to distinguish the orthogonal pictures represented by $\mathcal{N} = 4$ SYM theory and kinetic theory. This is clearly an important goal and we refer to Ref.[10] for theoretical background. Also throughout this review we have emphasized the shear viscosity and neglected bulk viscosity. This is because on the hadronic side of the phase transition the bulk viscosity is a thousand times smaller than the shear viscosity in the regime where it can be reliably calculated [100]. Similarly on the QGP side of the phase transition the bulk viscosity is a thousand times smaller than the shear viscosity [101]. However near a second order phase transition the bulk viscosity can become very large [103,16,102]. Nevertheless the rapid cross-over seen in Fig. 8 is not particularly close to a second order phase transition and universality arguments can be questioned (see Ref.[27] for a discussion in the context of chiral susceptibility.) Given the ambiguity at this moment it seems prudent to leave bulk viscosity to future review.

4. Hydrodynamic Description of Heavy Ion Collisions

In the previous sections we analayzed the phase diagram of QCD and esimated the transport coefficients in different phases. In this section we will study the hydrodynamic modelling of heavy ion collisons.

In Section 4.2 we will consider ideal hydrodynamics and assume that the mean free paths are small enough to support this interpretation. Subsequently we will study viscous hydrodynamics in Section 4.3. Section 4.4 will analyze the ratio of the viscous terms to the ideal terms and use the estimates of the transport coefficients given above to asses the validity of the hydrodynamic interpretation. Section 4.6 will discuss the recent advances in intepreting the hydrodynamic equations beyond the Navier Stokes limit. This work will lay the foundation for the more detailed hydrodynamic models presented in Section 6.

4.1. *Ideal Hydrodynamics in Heavy Ion Collisions*

The stress tensor of an ideal fluid and its equation of motion are simply

$$T^{\mu\nu} = eu^\mu u^\nu + \mathcal{P}\Delta^{\mu\nu}\,, \qquad \partial_\mu T^{\mu\nu} = 0\,. \tag{28}$$

where e is the energy density and $\mathcal{P}(e)$ is the pressure. Here we will use the metric $(-,+,+,+)$ and define the projection tensor, $\Delta^{\mu\nu} = g^{\mu\nu} + u^\mu u^\nu$. This decomposition of the stress tensor is simply a reflection of the fact that in the local rest of a thermalized medium the stress tensor must have the form, $\mathrm{diag}(e, \mathcal{P}, \mathcal{P}, \mathcal{P})$. In developing viscous hydrodynamics we will define two derivatives which are the time D, and spatial derivatives ∇^μ in the local rest frame

$$D \equiv u^\mu \partial_\mu\,, \qquad \nabla^\mu \equiv \Delta^{\mu\nu}\partial_\mu\,. \tag{29}$$

The ideal equations of motion can be written

$$De = -(e+\mathcal{P})\nabla_\mu u^\mu\,, \tag{30}$$

$$Du^\mu = -\frac{\nabla^\mu \mathcal{P}}{e+\mathcal{P}}\,. \tag{31}$$

The first equation says that the change in energy density is due to the $\mathcal{P}dV$ work or equivalently that entropy is conserved. To see this we assosciate $\nabla_\mu u^\mu$ with the fractional change in volume per unit time, $dV/V = dt \times \nabla_\mu u^\mu$, and use the thermodynamic identity, $d(eV) = Td(sV) - \mathcal{P}dV$. The second equation says that the acceleration is due to the gradients of pressure. The enthalpy plays the role of the mass density in a relativistic theory. Notice that hydrodynamics does not depend on possible (divergent) vacuum contributions to the pressure; it involves only pressure gradients and the enthalpy.

4.2. *Ideal Bjorken Evolutions and Three Dimensional Estimates*

In this section we will follow an analysis due to Bjorken [81] and apply ideal hydrodynamics to heavy ion collisions. Bjorken's analysis was subsequently extended in important ways [82,56,83]. In high energy heavy ion collision the two nuclei pass through each other and the partons are scarcely stopped. This statement underlies much of the interpretation of high energy events and an enormous amount of data is consistent with this assumption. For a time which is short compared to the transverse size of the nucleus, the transverse expansion can be ignored.

Given that the nuclear constituents pass through each other, the longitudinal momentum is much much larger than the transverse momentum. Because of this scale separation there is a strong identification between the space-time coordinates and the typical z momentum. For example a particle with typical momentum p_z and energy E will be found in a definite region of space time

$$v^z = \frac{p^z}{E} \simeq \frac{z}{t}\,. \tag{32}$$

This kinematics is best analyzed with proper time and space-time rapidity variables, τ and η_s[a]

$$\tau \equiv \sqrt{t^2 - z^2}\,, \qquad \eta_s \equiv \frac{1}{2}\log\left(\frac{t+z}{t-z}\right)\,.$$

At a proper time τ particles with rapidity y are predominantly located at space time rapidity η_s

$$y \equiv \frac{1}{2}\log\frac{p_z + E}{E - p_z} \simeq \frac{1}{2}\log\frac{t+z}{t-z} \equiv \eta_s \tag{33}$$

Fig. 10 illustrates these coordinates and shows schematically the indentification between η_s and y. At an initial proper time τ_o, in each space time rapidity slice there is a collection of particles predominantly moving with four velocity u^μ.

$$\frac{1}{2}\log\left(\frac{u^0 + u^z}{u^0 - u^z}\right) \simeq \eta_s \tag{34}$$

The beam rapidity at RHIC is $y_{\rm beam} \simeq 5.3$ and therefore roughly speaking the particles are produced in the space-time rapidity range $-5.3 < \eta_s < 5.3$. It is important to realize that (up to about a unit or so) each space-time rapidity slice is associated with a definite angle in the detector. For ultra-relativistic particles $E \simeq p$ we have

$$\eta_s \simeq y \simeq \frac{1}{2}\log\left(\frac{p + p_z}{p - p_z}\right) = \frac{1}{2}\log\left(\frac{1+\cos\theta}{1-\cos\theta}\right) \equiv \eta_{\rm pseudo} \tag{35}$$

where a particular θ is shown in Fig. 1. Bjorken used these kinematic ideas to estimate initial energy density in the $\eta_s = 0$ rapidity slice at an initial time, $\tau_o \simeq 1\,\text{fm}$. The estimate is based on fairly well supported assumption that the energy which finally flows into the detector $\frac{dE_T}{d\eta_{\rm pseudo}}$ largely reflects the initial energy in a given space-time rapidity slice

$$\epsilon_{Bj} \simeq \frac{1}{A}\frac{\Delta E}{\Delta z} \simeq \frac{1}{\tau_o}\frac{\Delta E}{\Delta \eta_s} \simeq \frac{1}{A\tau_o}\frac{dE_\perp}{d\eta_{\rm pseudo}} \tag{36}$$

$$\simeq 5.5\frac{\rm GeV}{\rm fm^3} \tag{37}$$

In the last line we have estimate the area of a gold nucleus as $A \simeq 100\,\text{fm}^2$ and taken $\tau_o \simeq 1\,\text{fm}$ and used the measured $dE_T/d\eta \simeq 6.4\text{GeV} \times N_p$ where $N_p \simeq 340$ is the number of participants [15]. The estimate is generally considered a lower limit since during the expansion there is $\mathcal{P}dV$ work as the particles in one rapidity slice push agains the particles in another rapidity slice [56,82,83] (See Fig. 10). Using the equation of state in Fig. 8 we estimate an initial temperature $T(\tau_o) \simeq 250\,\text{MeV}$. As mentioned above this estimate is somewhat low for hydrodynamic calcluations

[a]Here η_s denotes the space time rapidity, $\eta_{\rm pseudo}$ denotes the psuedo-rapidity (see below), η denots the shear viscosity. In raised space time indices in τ, η_s coordinates we will omit the "s" when confusion can not arise, *e.g.* $\pi^{\eta\eta} = \pi^{\eta_s\eta_s}$.

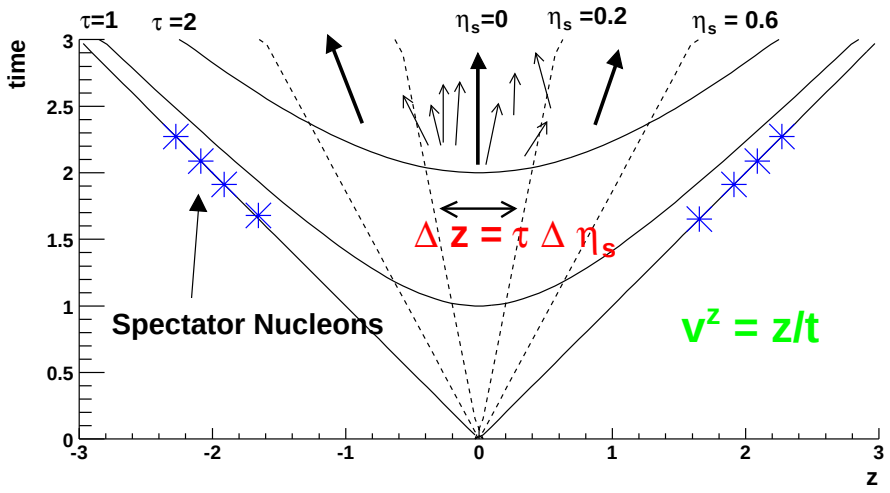

Fig. 10. A figure motivating for the Bjorken model. The space between the dashed lines of constant η_s are referred to as a space-time rapidity slice in the text. Lines of constant proper time τ are given by the solid hyperbolas. The collection of particles in the $\eta_s = 0$ rapidity slice is indicated by the small arrows for the central ($\eta_s = 0$) rapidity slice only. The solid arrows indicates the average four velocity u^μ in each slice. The spectators are those nucleons which do not participate in the collision and lie algong the light cone.

and a more typical temperature is $T \simeq 310\,\mathrm{MeV}$, which has the roughly twice the Bjorken energy density, [13].

The distribution of the energy density $e(\tau_o, \eta)$ at τ_o in space-time rapidity slice is not necessarily uniform. In the color glass picture for instance, the final distribution of multiplicity is related to the x distribution of partons inside the nucleus [80]. Bjorken made the additional simplifying assumption that the energy density is uniform in space-time rapidity, *i.e.* $e(\tau_o, \eta) \simeq e(\tau_o)$. With this simplification, the identification between the fluid and space time rapidities remains fixed as the fluid flows into the forward light cone.

We have discussed the motivation for the Bjorken model. Formally the model consists of the following ansatz for the hydrodynamic variables

$$e(t, \mathbf{x}) = e(\tau) \qquad u^\mu(t, \mathbf{x}) = (u^0, u^x, u^y, u^z) = (\cosh(\eta_s), 0, 0, \sinh(\eta_s))\,. \tag{38}$$

We will use curvlinear coordinates where

$$x^\mu = (\tau, \mathbf{x}_\perp, \eta_s) \qquad g_{\mu\nu} = \mathrm{diag}(-1, 1, 1, \tau^2) \qquad (u^\tau, u^x, u^y, u^\eta) = (1, 0, 0, 0)\,.$$

Substituting this ansatz into the conservation laws yields the following equation for the energy density

$$\frac{de}{d\tau} = -\frac{e + \mathcal{P}}{\tau}\,. \tag{39}$$

The energy per unit space-time rapidity (τe) decreases due to the $\mathcal{P}dV$ work.

This equation can be solved for a massless ideal gas equation of state and the time dependence of the temperature is

$$T(\tau) = T_o \left(\frac{\tau_o}{\tau}\right)^{1/3} , \tag{40}$$

where T_o is the initial temperature. The temperature decreases rather slowly as a function of proper time during the initial one dimensional expansion. This will turn out to be important when discussing equilibration. For a massless ideal gas, the entropy is $s \propto T^3$ and decreases as

$$s(\tau) = s_o \frac{\tau_o}{\tau} . \tag{41}$$

Now we discuss what happens when the initial energy density the distribution is not uniform rapidity. Due to pressure gradients in the longitudinal direction, there is some longtidunal acceleration This changes the strict identification between the space time rapidity and the fluid rapidity given in Eq. (34). It also changes the temperature dependence given above. One way to quantify this effect is to look at the results of 3D ideal hydrodynamic calculations and study the differences between the initial energy distribution $\int d^2\mathbf{x}_\perp \, e(\tau_o, \mathbf{x}_\perp, \eta)$ and the final energy distribution $\int d^2\mathbf{x}_\perp \, e(\tau_f, \mathbf{x}_\perp, \eta)$. Generally, the final distribution in space-time rapidity is similar to the initial distribution in space-time rapidity [51,50]. Therefore, the effect of longitudinal acceleration is unimportant until late times.

The nuclei have a finite transverse size $R_{\rm Au} \sim 6\,{\rm fm}$. After a time of order

$$\tau \sim \frac{R_{\rm Au}}{c} ,$$

the expansion becomes three dimensional. To estimate how the temperature evolves during the course of the resulting three dimensional expansion, consider a sphere of radius R which expands in all three directions. The radius and volume increase as

$$R \propto \tau \qquad V \propto \tau^3 .$$

Since for an ideal expansion the total entropy in the sphere is constant, the entropy density decreases as $1/\tau^3$ and the temperature decreases as

$$s \propto \frac{1}{\tau^3} , \qquad T \propto \frac{1}{\tau} . \tag{42}$$

Here we have estimated how the entropy decreases during a one and three dimensional expansion of an ideal massless gas. Now if during the course of the collision there are non-equilibrium processes which generate entropy that ultimately equilibrates, the temperature of this final equilibrated gas will be larger than if the expansion was isentropic. Effectively the temperature will decrease more slowly. To estimate this effect in a one dimensional expansion, we imagine a free streaming gas where the longitudinal pressure is zero. Then from Eq. (39) we have

$$\frac{de}{d\tau} \sim \frac{e}{\tau} . \tag{43}$$

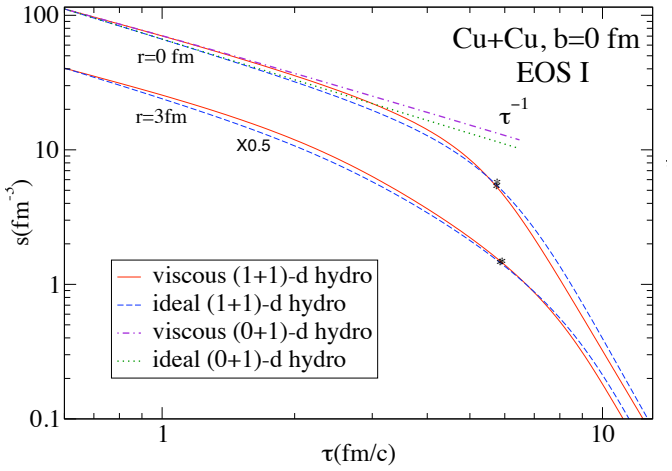

Fig. 11. Figure from Ref.[79] showing the entropy density s in CuCu simulations as a function of proper time τ using ideal and viscous hydrodynanics. During an initial one dimensional the entropy density decreases as $s \propto 1/\tau$. Subsequently the entropy decreases as $s \propto 1/\tau^3$ when the expansion becomes three dimensional at a time, $\tau \sim 5\,\mathrm{fm}$. The lines indicated by $(0+1)$ ideal and $(0+1)$ viscous are representative of the ideal and viscous Bjorken results Eq. (39) and Eq. (50) respectively.

In the sense discussed above, this equation may be integrated to estimate that the temperature and entropy decrease as

$$T \propto \frac{1}{\tau^{1/4}}\,, \qquad s \propto \frac{1}{\tau^{3/4}}\,. \tag{44}$$

Similarly in a three dimensional expansion we can estimate how entropy production will change the powers given in Eq. (42). Again consider a sphere of radius R which expands in all three directions, such that $R \propto \tau$ and $V \propto \tau^3$. For a free expansion without pressure the total energy in the sphere is constant, and the energy density decreases as $1/\tau^3$. Similarly, we estimate that the temperature and entropy density decrease as

$$T \propto \frac{1}{\tau^{3/4}}\,, \qquad s \propto \frac{1}{\tau^{9/4}}\,. \tag{45}$$

In summary we have estimated how the temperature and entropy density depend on the proper time τ during the course of an ideal and non-ideal $1D$ and $3D$ expansion. This information is recorded in Table 1. These estimates are also nicely realized in actual hydrodynamic simulations. Fig. 11 shows the dependece of entropy density as a function of proper time τ. The figure indicates that the entropy decreases as $1/\tau$ during an initial one dimensional expansion and subsequently decreases as $1/\tau^3$ when the expansion becomes three dimensional at a time of order

Quantity	1D Expansion	3D Expansion
T	$\left(\frac{1}{\tau}\right)^{1/3\div 1/4}$	$\left(\frac{1}{\tau}\right)^{1\div 3/4}$
$s \propto T^3$	$\left(\frac{1}{\tau}\right)^{1\div 3/4}$	$\left(\frac{1}{\tau}\right)^{3\div 9/4}$

Table 1. Dependence of temperature and entropy as a function of time in a 1D and 3D expansion. The indicated range, for instance $1/3 \div 1/4$, is an estimate of how extreme non-equilibrium effects could modify the ideal power from 1/3 to 1/4.

$\sim 5\,\mathrm{fm}$. These basic estimates will be useful when estimating the relative size of viscous terms in what follows.

4.3. *Viscous Bjorken Evolution and Three Dimensional Estimates*

This section will analyze viscosity in the context of the Bjorken model with the primary goal of assesing the validity of hydrodynamics in heavy ion collisons. In viscous hydrodynamics the stress tensor is expanded in all possible gradients of the conserved changes. Using lower order equations of motion any time derivatives of conserved quantities can be rewritten as spatial derivatives. The stress tensor can be decomposed into ideal and viscous pieces

$$T^{\mu\nu} = T^{\mu\nu}_{\text{ideal}} + \pi^{\mu\nu} + \Pi\Delta^{\mu\nu}\,, \tag{46}$$

where $T^{\mu\nu}_{\text{id}}$ is the ideal stress tensor (Eq. (28)) and Π is the bulk stress. $\pi^{\mu\nu}$ is symmetric traceless shear stress tensor and satisfies the orthogonality constraint, $\pi^{\mu\nu}u_\mu = 0$. The equations of motion are the conservation laws $\partial_\mu T^{\mu\nu} = 0$ together with a constituent relation. The constituent relation expands $\pi^{\mu\nu}$ and Π in terms gradients of conserved charges T^{00} and T^{0i} or their thermodynamic conjugates, temperature T and four velocity u^μ . To first order in this expansion, the equations of motion and the constituent relation are

$$\partial_\mu T^{\mu\nu} = 0\,, \qquad \pi^{\mu\nu} + \Pi\Delta^{\mu\nu} = -\eta\sigma^{\mu\nu} - \zeta\nabla_\mu u^\mu\,, \tag{47}$$

where η and ζ are the shear and bulk viscosities respectively, and we have defined

$$\sigma^{\mu\nu} = \nabla^\mu u^\nu + \nabla^\nu u^\mu - \frac{2}{3}\Delta^{\mu\nu}\nabla_\lambda u^\lambda\,. \tag{48}$$

For later use we also define the bracket $\langle\ldots\rangle$ operation

$$\langle A^{\mu\nu}\rangle \equiv \frac{1}{2}\Delta^{\mu\alpha}\Delta^{\nu\beta}\left(A_{\alpha\beta} + A_{\beta\alpha}\right) - \frac{1}{3}\Delta^{\mu\nu}\Delta^{\alpha\beta}A_{\alpha\beta}\,, \tag{49}$$

which takes a tensor and renders it symmetric, traceless and orthogonal to u^μ. Note that $\sigma^{\mu\nu} = 2\langle\partial^\mu u^\nu\rangle$.

We now extend the Bjorken model to the viscous case following Ref.[56]. The bulk viscosity is neglected in the following analysis and we refer to Section 3 for a more complete discussion. Substituting the Bjorken ansatz (Eq. (38)) into the

conservation laws and the associated constituent relation (Eq. (47)), yields the time evolution of the energy density

$$\frac{de}{d\tau} = -\frac{e + \mathcal{P} - \frac{4}{3}\eta/\tau}{\tau}\,. \tag{50}$$

The system is expanding in the z direction and the pressure in the z direction is reduced from its ideal value. Formally this arises due to the gradient $\partial_z u^z = 1/\tau$ and the constituent relation Eq. (47)

$$T^{zz} = \mathcal{P} - \frac{4}{3}\frac{\eta}{\tau}\,. \tag{51}$$

4.4. *The applicability of hydrodynamics and η/s*

We have written down the viscous Bjorken model. Comparing the viscous equation of motion Eq. (50) to the ideal equation of motion Eq. (39), we see that the hydrodynamic expansion is controlled by

$$\frac{\eta}{e+p}\frac{1}{\tau} \ll 1\,. \tag{52}$$

This is a very general result and is a function of time and temperature. Using the thermodynamic relation $e + p = sT$, we divide this condition into a constraint on a medium parameter η/s and a constraint on an experimental parameter $1/\tau T$

$$\underbrace{\frac{\eta}{s}}_{\text{medium parameter}} \quad \times \quad \underbrace{\frac{1}{\tau T}}_{\text{experimental parameter}} \quad \ll 1\,. \tag{53}$$

If the experimental conditions are favorable enough, it is appropriate to apply hydrodynamics regardless of the value of η/s. This is the case for sound waves in air where although η/s is significantly larger than the quantum bound, but hydrodynamics remains a good effective theory. However, for the application to heavy ion collisions, the experimental conditions are so unfavorable that only if η/s is close to the quantum bound will hydrodynamics be an appropriate description.

For instance, in heavy ion collision we estimated the experimental condition in Section 4.1

$$\frac{1}{\tau_o T_o} = 0.66 \left(\frac{1\,\text{fm}}{\tau_o}\right)\left(\frac{300\,\text{MeV}}{T_o}\right)\,. \tag{54}$$

Here we have evaluated this experimental parameter at a specific initial time τ_o and will discussion of the time evolution in the next section. In Section 3 estimated the medium parameter η/s and can now place these results in context

$$0.2 \left(\frac{\eta/s}{0.3}\right)\left(\frac{1\,\text{fm}}{\tau_o}\right)\left(\frac{300\,\text{MeV}}{T_o}\right) \ll 1\,. \tag{55}$$

Thus hydrodynamics will begin to be a good approximation for $\eta/s \lesssim 0.3$ or so. This estimate is born out by the more detailed calculations presented in Section 6.

Reexamining Fig. 9, we see that the value of $\eta/s \simeq 0.3$ is at the low end of the perutrbative QGP estimates given in the figure and it is difficult to reconcile the observation of strong collective flow with a quasi-particle picutre of quarks and gluons. Thus the estimates of η/s coming from the RHIC experiments, which are based on the hydrodynamic interpretation of the observed flow, should be accepted only with considerable care.

4.5. *Time Evolution*

In the previous section we have estimated the relevance of hydrodynamics at a time $\tau_o \approx 1\,\mathrm{fm}$. In this section we will estimate (again using hydrodynamics) how the size of the viscous terms depends on time. For this purpose we will keep in mind a kinetic theory estimate for the shear viscosity

$$\eta \sim \frac{T}{\sigma_o}\,, \tag{56}$$

and estimate how the gradient expansion parameter in Eq. (50) depends on time.

First consider a theory where the temperature T is the only scale and also consider a 1D Bjorken expansion. The shear viscosity is proportional to T^3 and the entropy scales as T^3 so the hydrodynamic expansion parameter scales as

$$\frac{\eta}{(e+p)}\frac{1}{\tau} \sim \frac{1}{\tau T} \sim \frac{1}{\tau^{2/3}}\,. \tag{57}$$

In the last step we have used the fact that for a scale invariant gas undergoing an ideal Bjorken expansion the temperature decreases as $1/\tau^{1/3}$. In general if we have some non equilibrium processes which produce entropy during the course of the expansion, the temperature will decrease more slowly than estimated in the ideal gas case. This was estimated above and is recorded in Table 1. The result is that we do not expect the temperature (or more properly some typical momentum scale as a function of time) to decrease more slowly than $1/\tau^{1/4}$, and we can estimate that the hydrodynamic expansion parameter evolves as

$$\frac{\eta}{(e+p)}\frac{1}{\tau} \propto \frac{1}{\tau T} \propto \frac{1}{\tau^{2/3\div 3/4}}\,. \tag{58}$$

Compare this scale invariant conformal gas, to a gas with a very definite cross section σ_o. There are clearly important scales in the quark gluon plasma as the medium approaches the transition point. For instance spectral densities of current-current correlators near the point show a very discernible correlation near where the ρ meson will form in the hadron phase [59,58,11]. Thus the intent of studying this extreme limit with constant cross section is show some of the possible effects of these scales. Further the constant cross section kinetic theory is often used in arguments regarding the impact parameter dependence of elliptic flow [57].

For a constant cross section gas the hydrodynamic expansion parameter evolves as

$$\frac{\eta}{(e+p)}\frac{1}{\tau} \propto \frac{1}{s\sigma\tau} \propto \tau^{0\div 1/4}\,. \tag{59}$$

Thus, a gas with a constant cross section undergoing a one dimensional isentropic expansion will move neither away nor toward equilibrium as a function of time. Non-equilibrium effects will make the matter evolve slowly toward equilibrium.

Now we will compute the analogous effects for a three dimensional expansion. In the conformal case $\eta \propto T^3$ and $T \propto \frac{1}{\tau}$, so that the final result is

$$\frac{\eta}{(e+p)}\frac{1}{\tau} \propto \frac{1}{\tau T} \propto \left(\frac{1}{\tau}\right)^{0\div 1/4} . \tag{60}$$

Thus a conformal gas expanding in three dimensions moves neither away nor towards equilibrium. Similarly for gas with a constant cross section the hydrodynamic parameter evolves as

$$\frac{\eta}{(e+p)}\frac{1}{\tau} \propto \frac{1}{s\sigma\tau} \propto \tau^{2\div 5/4} . \tag{61}$$

In estimating this last line we have use Table 1. Thus we see that a gas with fixed cross-sections which expands in three dimensions very rapidly breaks up.

The preceding results are summarized into Table 2. Essentially the heavy ion collision proceeds along the following line of reasoning. First, there is a one dimensional expansion where temperature (or "effective" temperature) is the dominant scale in the problem. The parameter which controls the applicability of hydrodynamics $\eta/[(e+p)\tau]$ decreases as a function of time; hydrodynamics gets better and better, evolving according to the upper left corner of Table 2. As the system expands and cools toward the transition region additional scales enter the problem. Typically at this point $\tau \sim 4\,\mathrm{fm/c}$ the expansion also becomes three dimensional. The system then enters the lower right corner of Table 2 and very quickly the nucleus nucleus collision starts to break up. We note that it is necessary to introduce some scale into the problem in order to see this freezeout process. For a conformal liquid with $\eta \propto T^3$ the system never freezes out even for a 3D expansion. This can be seen by looking at the upper-right corner of the table and noting that the hydrodynamic expansion parameter behaves as

$$\frac{\eta}{(e+p)\tau} \propto \left(\frac{1}{\tau}\right)^{0\div 1/4} , \tag{62}$$

and therefore approaches a constant (or slowly equilibrates) at late times. From this discussion we see that the temperature dependence of the shear viscosity ultimately is ultimately responsible for setting the duration of the hydrodynamic expansion.

4.6. *Second Order Hydrodynamics*

In first-order relativistic viscous hydrodynamics there are reported instabilities which are related to the treatment of the gradient expansion [86]. In the first-order theory, the stress tensor is instantly specified by the constituent relation and this leads to acausal propagation [87]. Nevertheless, it was generally understood that one

Model	1D Expansion	3D Expansion
$\eta \propto T^3$	$\frac{\eta}{(e+p)\tau} \propto \left(\frac{1}{\tau}\right)^{2/3 \div 3/4}$	$\frac{\eta}{(e+p)\tau} \propto \left(\frac{1}{\tau}\right)^{0 \div 1/4}$
$\eta \propto \frac{T}{\sigma_o}$	$\frac{\eta}{(e+p)\tau} \propto \left(\frac{1}{\tau}\right)^{0 \div 1/4}$	$\frac{\eta}{(e+p)\tau} \propto \tau^{2 \div 5/4}$

Table 2. Dependence of the hydrodynamic expansion parameter $\eta/[(e+p)\tau]$ as a function of time for two different functional forms for η ($\eta \propto T$ and $\eta \propto T^3$) and two expansion types (1D and 3D). A range of powers is given; the first power corresponds to ideal hydrodynamics and the second power corresponds to an estimate of non-equilibrium evolution.

could write down any model relaxation model which conserved energy and momentum, which included some notion of entropy, and the results of such a model would be indistinguishable from the Navier Stokes equations [114,96,95]. Many hydrodynamic models were written down [90,91,92,93,94] starting with a model by Israel and Stewart [89,90] and Müller [85]. For example in the authors own work the strategy was to write down a fluid model (based on Ref.[93]) which relaxed on some time scale to the Navier Stokes equations, solve these model equations on the computer, and finally to verify that the results are independent of the details of the model [73]. Thus the goal was to solve the Navier Stokes equations and to estimate the effects of higher order terms.

Recently an important work by R. Baier, P. Romatschke, D. T. Son, A. O. Starinets and M. A. Stephanov (hereafter BRSSS) clarified and classified the nature of these higher order terms [75]. An important impetus for this work came from the AdS/CFT correspondence [75,76,77]. Many of the fluid models discussed above were motivated by kinetic theory. However in the strongly coupled $\mathcal{N} = 4$ Super Yang Mills plasma kinetic theory is not applicable and the precise meaning of these models was vague. BRSSS determined precisely in what sense these second order viscous equations are theories and in what sense they are models. The Tatta group completed the calculation of the second order transport coefficients in $\mathcal{N} = 4$ SYM theory and clarified the hydrodynamic nature of black branes in the process [76].

The spirit of the BRSSS analysis is the following:

(1) Write the stress tensor as an expansion in all possible second order gradients of conserved charges which are allowed by the symmetries with arbitrary coefficients.
(2) In general one may use lower order equations of motion to rewrite the temporal derivatives of conserved quantities into spatial derivatives.
(3) The resulting equation of motion $\partial_\mu T^{\mu\nu} = 0$ for the conserved charges will be able to match or reproduce all retarded correlators of the full microscopic calculation by adjusting the coefficients of the gradient expansion.

In general, for a theory with conserved baryon number there are many terms. By focusing on a theory without baryon number and also assuming that the fluid is

conformally invariant, the number of possible second order terms is relatively small. The classification of gradients in terms of there conformal transformation properties was very useful, both theoretically and phenomenologically. At a theoretical level there are a managable number of terms to write down. At a phenomenological level it is the gradient expansion converges more rapidly when only those second order terms which are allowed by conformal invariance are included (see Section 6). Subsequently when additional conformal breaking terms are added the conformal classification provides a useful estimate for the size of these terms, *i.e.* quantities that scale as $T^\mu_\mu = e - 3p$ should be estimated differently than those that scale as energy density itsself. In retrospect, this classification is an "obvious" generalization of the first order Navier-Stokes equations.

Proceding more technically, in analogy to the constituent relation of the Navier-Stokes theory Eq. (47), BRSSS determine that the possible forms of the gradient expansion in a conformal liquid are

$$\begin{aligned}\pi^{\mu\nu} = &-\eta\sigma^{\mu\nu} + \eta\tau_\pi \left[\langle D\sigma^{\mu\nu}\rangle + \frac{1}{d-1}\sigma^{\mu\nu}\partial\cdot u\right] \\ &+\lambda_1 \left\langle \sigma^\mu{}_\lambda \sigma^{\nu\lambda}\right\rangle + \lambda_2 \left\langle \sigma^\mu{}_\lambda \Omega^{\nu\lambda}\right\rangle + \lambda_3 \left\langle \Omega^\mu{}_\lambda \Omega^{\nu\lambda}\right\rangle ,\end{aligned} \tag{63}$$

where the vorticity tensor is defined as

$$\Omega^{\mu\nu} = \frac{1}{2}\Delta^{\mu\alpha}\Delta^{\nu\beta}\left(\partial_\alpha u_\beta - \partial_\beta u_\alpha\right) . \tag{64}$$

and $d = 4$ is the number of space-time dimensions. We note for the reader that ∇^μ in BRSSS denoted covariant derivative rather than the spatial derivative $\nabla^\mu = \Delta^{\mu\nu}\partial_\nu$ defined here. Conformal invariance forces a particular combination of gradients to have a single coefficient

$$\tau_\pi \left[\langle D\sigma^{\mu\nu}\rangle + \frac{1}{d-1}\sigma^{\mu\nu}\partial\cdot u\right] \tag{65}$$

The time derivative $D\sigma^{\mu\nu}$ may be expanded out using lower order equations of motion if desired. The constituent relation in Eq. (63) together with the conservation law are the second order equations of motion of a conformal fluid. They are precisely analogous to the first order theory. As in the first order case, these equations are also acausal.

To circumvent this issue, BRSSS (following the spirit of earlier work by Israel and Stewart [89,90] and Müller [85]) promote the constituent relation to a dynamical equation for the viscous components of the stress tensor $\pi^{\mu\nu}$. Using the lower order relation $\pi^{\mu\nu} = -\eta\sigma^{\mu\nu}$, the (conformal) dependence of η on temperature $\eta \propto T^{d-1}$, and the ideal equation of motion Eq. (30), the following equation of motion arises for $\pi^{\mu\nu}$

$$\begin{aligned}\pi^{\mu\nu} = &-\eta\sigma^{\mu\nu} - \tau_\pi \left[\langle D\pi^{\mu\nu}\rangle + \frac{d}{d-1}\pi^{\mu\nu}\nabla\cdot u\right] \\ &+\frac{\lambda_1}{\eta^2}\left\langle \pi^\mu{}_\lambda \pi^{\nu\lambda}\right\rangle - \frac{\lambda_2}{\eta}\left\langle \pi^\mu{}_\lambda \Omega^{\nu\lambda}\right\rangle + \lambda_3 \left\langle \Omega^\mu{}_\lambda \Omega^{\nu\lambda}\right\rangle .\end{aligned} \tag{66}$$

From a numerical perspective the resulting equation of motion is now frist order in derivatives, hyperbolic and causal. The modes in this (and similar) models have been studied in Refs.[95,87,75]

Nevertheless it should be empasized that the domain of validity of the resulting equations is still the same as Eq. (63), *i.e.* the hydrodynamic regime. Thus for instance the second order equations should be used in a regime where

$$|-\pi^{\mu\nu} + \eta\sigma^{\mu\nu}| \ll |\eta\sigma^{\mu\nu}| \,.$$

Outside of this regime there is no guarantee that entropy production predicted by this model will be positive during the course of the evolution [75]. It should also be emphasized that this is not a unique way to construct a hydrodynamic model which reduces to Eq. (63) in the long wavelength limit – see Ref.[10] for an example discussed in these terms. What is guaranteed is that any conformal model or dynamics (such as conformal kinetic theory [8,9] or the dynamics predicted by AdS/CFT [75,76]) will in the long wavelength limit be expressible in terms of the gradient expansion given above.

There is an important distinction between the first and second order theories [114,10,96]. In the first order theory, the ideal motion is damped, and there are corrections to the ideal motion of order

$$\frac{\eta}{(e+p)L^2}\Delta t \,,$$

where L is the characteristic spatial dimension of the system and Δt is the time of observation. Thus for sufficiently long times the viscous corrections become large and must be ressummed by solving the Navier-Stokes equations. Once this is done however, the remaining higher order terms (which are captured by the second order theory) are *uniformly* small and modify the Navier-Stokes solution by an amount of order

$$\ell^2_{\rm mfp}/L^2 \,.$$

Often this makes these higher order terms difficult to measure in normal laboratory liquids [10].

For completeness we record the model equations which have been discussed in the heavy ion litterature [72,78,79,69].

(1) The first of these is the simplified Israel-Stuart equation,

$$\pi^{\mu\nu} = -\eta\sigma^{\mu\nu} - \tau_\pi \langle D\pi^{\mu\nu}\rangle \,. \tag{67}$$

Since the derivatives do not appear as the combination

$$\langle D\pi^{\mu\nu}\rangle + \frac{d}{d-1}\pi^{\mu\nu}\nabla\cdot u \,, \tag{68}$$

but rather involve $\langle D\pi^{\mu\nu}\rangle$, this model does not respect conformal invariance.

Quanity	$\mathcal{N}=4$ SYM	QCD Kinetic Theory	Relaxation Time
$\eta\tau_\pi$	$4-2\ln(2)\simeq 2.61$	5.9 to 5.0 (due to g)	6
λ_1	2	5.2 to 4.1 (due to g)	6 ($\equiv \eta\tau_\pi$)
λ_2	$-4\ln(2)\simeq -2.77$	-11.8 to -10 ($\equiv -2\eta\tau_\pi$)	-12 ($\equiv -2\eta\tau_\pi$)
λ_3	0	0	0

Table 3. Compliation of values of (rescaled) second order transport quantitites $(\eta\tau_\pi, \lambda_1, \lambda_2, \lambda_3)$. *All* numbers in this table should be *multiplied* by $\eta^2/(e+\mathcal{P})$. The complete strong coupling results are from an amalgamation Ref.[75] and Ref.[76]. The weak coupling results are from Ref.[8] and the relaxation time approximation was studied in Ref.[75] and clarified in Ref.[8]. Hydrodynamic simulations of the heavy ion event are not sensitive to these values.

(2) The second model is the full Israel-Stewart equation which has the following form [99]

$$\pi^{\mu\nu} = -\eta\sigma^{\mu\nu} - \tau_\pi \langle D\pi^{\mu\nu}\rangle + \frac{1}{2}\pi^{\mu\nu}\frac{\eta T}{\tau_\pi}\partial_\rho\left(\frac{\tau_\pi}{\eta T}u^\rho\right) + 2\tau_\pi\,\pi^{\alpha(\mu}\Omega^{\nu)}{}_\alpha\,, \quad (69)$$

$$\to -\eta\sigma^{\mu\nu} - \tau_\pi\left[\langle D\pi^{\mu\nu}\rangle + \frac{d}{d-1}\pi^{\mu\nu}\nabla\cdot u\right] + 2\tau_\pi\,\pi^{\alpha(\mu}\Omega^{\nu)}{}_\alpha\,. \quad (70)$$

In the last line we have used the conformal relation, $\eta T/\tau_\pi \propto T^{d+1}$ and equation of motion, $D(\ln T) = -1/(d-1)\nabla\cdot u$. The model is equivalent to taking $\lambda_1=\lambda_3=0$ and $\lambda_2=-2\eta\tau_\pi$.

There has been some effort to compute these coefficients both at strong and weak coupling. The gradient expansion in Eq. (63) implies that the relative size of the coefficients $(\ell_{\rm mfp}/L)^2$ which in a relativistic theory is of order $[\eta/(e+p)]^2$. The strong coupling results are listed in Table 4.6 and derivation of results clarified the hydrodynamic approximation in gauge gravity duality [76]. At weak coupling the results of detailed kinetic calculations are [8] (see also Ref.[9]) are also listed in the table. In kinetic theory the physics of these terms is the following: (1) The τ_π and λ_2 are a result of streaming of the first viscous correction $P^\mu\partial_\mu f_1$. The common origin of these terms ultimately explains their common value. (2) The contribution to the λ_1 (the visco-elastic $\pi\pi$ term) reflects the streaming $P^\mu\partial f_1$ *and* the non-linearities of the collision integral. (3) Finally the vorticity-vorticity term does not appear on the LHS of the Boltzman equation and therefore this term vanishes in kinetic theory [75,9,8]. In the strong coupling limit the absence of a vorticity-vorticity coupling is not understood.

In the relaxation time approximation discussed in Section 5 (with $\tau_R \propto E_{\mathbf{p}}$) the coefficient τ_π is readily calculated with linearized kinetic theory for a massless gas

$$\frac{(e+\mathcal{P})\eta\tau_\pi}{\eta^2} = 6\,, \tag{71}$$

The kinetic thoery relations $\lambda_2 = -2\eta\tau_\pi$ and $\lambda_3 = 0$ are respected for the same reasons as the full theory. Also in the relaxation time approximation approximation one finds $\lambda_1 = \eta\tau_\pi$ This relation which is not respected by the full kinetic theory since the non-linear terms in the collision integral are not captured by the linear relaxtion time approximation. Nevertheless, the relation almost holds indicating the dominance of the streaming term. Overall relaxation time approximation provides a good first estimate of these coefficients.

From a practical perspective a majority of simulations have used the full Israel-Stewart equations[72,78,70] and treated τ_π as a free parameter, varying $[\eta/(e+p)\tau_\pi]$ down from the relaxation time value by a factor of two. While it is gratifying that higher order transport coeffcients can be computed and classified, the final phenomenological results (see Section 6) are insensitive to the precise value of all second order terms for $\eta/s \lesssim 0.3$ [74,78,73]. Thus, the full hydrodynamic simulations corroborate the estimate given in Section 4.4 for the range of validity of hydrodynamics.

5. Kinetic Theory Description

In Section 4 we discussed various aspects of viscous hydrodynamics as applied to heavy ion collisions. Since ultimately the experiments measure particles, there is a need to convert the hydrodynamic information into particle spectra. This section will provide an introduction to the matching between the kinetic and hydrodynamic descriptions. This will be important when comparing the hydrodynamic models to data in Section 6. In addition, Section 3 discussed various calculations of the shear viscosity in QCD. Also in this section we will sketch briefly how these kinetic calculations are performed. Good summaries of these set of steps are provided by Refs.[118,101,119].

In kinetic theory the spectrum of particles in a volume Σ is given by the Cooper-Frye formula[112]

$$E\frac{d^3N}{d^3p} = \frac{1}{(2\pi)^3}\int_\Sigma \mathrm{d}\Sigma_\mu p^\mu\, f(-P\cdot u)\,, \tag{72}$$

Note that when Σ is a three volume at fixed time, $d\Sigma_\mu = (\mathrm{d}V, 0, 0, 0)$, and this formula reduces to the traditional result. Four vectors are denoted with capitol letters $P^\mu = (E_{\mathbf{p}}, \mathbf{p})$, and the *equilibrium* distribution funciton is denoted with

$$n(-P\cdot u) = \frac{1}{\exp(-P\cdot u/T)\pm 1}\,. \tag{73}$$

We will also use a suffix notation, $n_{\mathbf{p}} = n(-P\cdot U)$ and $f_{\mathbf{p}} = f(-P\cdot u)$. The

distribution function obeys the Boltzman equation

$$\partial_t f_{\mathbf{p}} + \frac{\mathbf{p}}{E_{\mathbf{p}}}\partial_x f_{\mathbf{p}} = -\int_{234} \Gamma_{12\to 34}\left(f_1 f_2 - f_3 f_4\right) , \tag{74}$$

where we have assumed $2 \to 2$ scattering and used classical statistics for simplicity, $f_{\mathbf{p}} = \exp(-E_{\mathbf{p}}/T)$. The momenta are labelled as $f_2 = f_{\mathbf{p}_2}$ and $f_1 = f_{\mathbf{p}_1}$ with $\mathbf{p}_1 \equiv \mathbf{p}$. The integral over the phase space is abbreviated

$$\int_{234} = \int \frac{d^3\mathbf{p}_2}{(2\pi)^3}\frac{d^3\mathbf{p}_3}{(2\pi)^3}\frac{d^3\mathbf{p}_4}{(2\pi)^3} , \tag{75}$$

and the transition rate $\Gamma_{12\to 34}$ for $2 \to 2$ scattering is related to the usual Lorentz invariant matrix element $|\mathcal{M}|^2$ as

$$\Gamma_{12\to 34} = \frac{|\mathcal{M}|^2}{(2E_1)(2E_2)(2E_3)(2E_4)}(2\pi)^4\delta^4(P_1 + P_2 - P_3 - P_4) . \tag{76}$$

The generalization of what follows to a multi-component gas and quantum statistics is left to the references[118].

During a viscous evolution the spectrum will be modified from its ideal form and this has important phenomenological consequences[71]

$$f = n_{\mathbf{p}} + \delta f . \tag{77}$$

The modification of the distribution function depends on the details of the microscopic interactions. In a linear approximation the deviation is proportional to the strains and can be calculated in kinetic theory. When the most important strain is shear, the deviation δf is propotional σ_{ij} . Traditionally we parametrize the viscous correction to the distribution in the rest frame of the medium [b]

$$\delta f_{\mathbf{p}} = -n_{\mathbf{p}}\,\chi(|\mathbf{p}|)\,\hat{\mathbf{p}}^i\hat{\mathbf{p}}^j\sigma_{ij} . \tag{78}$$

Then the stress tensor in the local rest frame at point $\mathbf{x}_o$

$$T^{ij} = p\delta^{ij} - \eta\sigma^{ij} = \int \frac{d^3\mathbf{p}}{(2\pi)^3}\frac{p^i p^j}{E_{\mathbf{p}}}\left[f_e + \delta f\right] \tag{79}$$

Substituting this form into the distribution function and using rotational symmetry we have

$$\eta = \frac{2}{15}\int \frac{d^3\mathbf{p}}{(2\pi)^3}\frac{p^2}{E_{\mathbf{p}}}\chi(|\mathbf{p}|)n_{\mathbf{p}} . \tag{80}$$

Thus we see that the form of the viscous correction to the distribution function determines the shear viscosity.

[b]When quantum statistics are taken into account this should be written

$$\delta f = -n_{\mathbf{p}}(1 \pm n_{\mathbf{p}})\,\chi(|\mathbf{p}|)\hat{\mathbf{p}}^i\hat{\mathbf{p}}^j\sigma_{ij} ,$$

where the overall minus is introduced because in the Navier-Stokes theory $\pi^{\mu\nu} = -\eta\sigma^{\mu\nu}$

To calculate the transport coefficients the Boltzman equaiton is analyzed in the rest frame of a particular location $\mathbf{x}_o$. In a neighborhood of this point the temperature and flow fields are

$$u^\mu(\mathbf{x},t) \simeq (1, u^i(\mathbf{x},t)) \qquad T(\mathbf{x},t) \simeq T_o + \delta T(\mathbf{x},t) \tag{81}$$

where $u^i(\mathbf{x}_o,t) = \delta T(\mathbf{x}_o,t) = 0$. The equlibrium distribution function in this neighborhood is

$$n(-P\cdot u) \simeq n^o_{\mathbf{p}} + n^o_{\mathbf{p}} \left(\frac{E_{\mathbf{p}}}{T_o^2}\,\delta T(\mathbf{x},t) + \frac{p^i u^i(\mathbf{x},t)}{T_o} \right), \tag{82}$$

where we have used the short hand notation $n^o_{\mathbf{p}} = \exp(-E_{\mathbf{p}}/T_o)$. We can now substitute the distribution function into the Boltzmann equation and find an equation the δf. The left hand side of the Boltzmann equation involes gradients, and therefore only the equilibrium distribution needs to be considered. Substituting Eq. (82) into the l.h.s. side of the Boltzmann equation using the ideal equations of motion,

$$\partial_t u^i = -\frac{\partial^i \mathcal{P}}{(e+\mathcal{P})} \tag{83}$$

$$\partial_t e = -(e+\mathcal{P})\partial_i u^i \tag{84}$$

and several thermodyanic relationships

$$c_v = \frac{de}{dT}\,, \tag{85}$$

$$\frac{n}{e+\mathcal{P}} d(\mu/T) = \frac{1}{T(e+\mathcal{P})} d\mathcal{P} + d\left(\frac{1}{T}\right) = 0\,, \tag{86}$$

we find that[c]

$$\partial_t f_e + v_{\mathbf{p}}\cdot\partial_{\mathbf{x}} f_e = \frac{n_{\mathbf{p}}}{E_{\mathbf{p}}} \left[\left(\frac{|\mathbf{p}|^2}{3T} - \frac{E^2_{\mathbf{p}}}{T}\frac{(e+\mathcal{P})}{Tc_v} \right) \partial_i u^i + \frac{p^i p^j}{2T}\sigma_{ij} \right]. \tag{87}$$

The result is proportional to two strains $\partial_i u^i$ and σ_{ij} which are ultimately responsible for the bulk and shear viscosity respectively. For a massless conformal gas we have $|\mathbf{p}|^2 = E^2_{\mathbf{p}}$, $Tc_v = 4e$ and $e + p = (4/3)e$. The result is that the term proportional to $\partial_i u^i$ vanishes and consequently the bulk viscosity is zero in this limit. We will subsequently only consider only the modifications due to the shear viscosity and refer to Section 3 for a more complete discussion.

In Eq. (87), the l.h.s. of the Boltzmann equation is evaluated at the point $\mathbf{x}_o$. We also evalaute the r.h.s. of the Boltzman equation at the point $\mathbf{x}_o$ to linear order in δf

$$n^o_{\mathbf{p}}\,\frac{p^i p^j}{2TE_{\mathbf{p}}}\sigma_{ij} = -\int_{234} \Gamma_{12\to 34}\, n^o_{\mathbf{p}} n^o_2 \left[\frac{\delta f(\mathbf{p})}{n^o_{\mathbf{p}}} + \frac{\delta f_2}{n^o_2} - \frac{\delta f_3}{n^o_3} - \frac{\delta f_4}{n^o_4} \right]. \tag{88}$$

[c]We have tacitly assumed that the dispersion curve does not depend on the temperature. This is fine as long as we are not considering the bulk viscosity [101].

In writing this equation we have made use of the detailed balance relation

$$n_1 n_2 \Gamma_{12\to 34} = n_3 n_4 \Gamma_{12\to 34}\,. \tag{89}$$

Eq. (88) should be regarded as a matrix equation for the distribution function $\delta f(\mathbf{p})$. Although $\delta f(\mathbf{p})$ or $\chi(p)$ can be determined numerically by straight forward discretization and matrix inversion, in practice a variational method is preferred [64,118]. After determining $\delta f(\mathbf{p})$ or $\chi(|\mathbf{p}|)$ the shear viscosity can be determined from Eq. (80).

This numerical work requires a detailed knowledge of the microscopic interactions. Lacking such detailed knowledge one can resort to a relaxation time approximation, writing the Boltzman equation as

$$\partial_t f + v_{\mathbf{p}}\cdot\partial_{\mathbf{x}} f = -\frac{1}{\tau_R(-P\cdot U)}\frac{(-P\cdot U)}{E_{\mathbf{p}}}\,\delta f \tag{90}$$

where $\tau_R(-P\cdot U)$ is a momentum dependent relaxation time. In the local rest frame this reduces to

$$\partial_t f + v_{\mathbf{p}}\cdot\partial_{\mathbf{x}} f = -\frac{1}{\tau_R(E_{\mathbf{p}})}\,\delta f\,. \tag{91}$$

By fiat the correction to the distribution function is simple

$$\delta f = -n_{\mathbf{p}}\frac{\tau_R(E_{\mathbf{p}})}{2TE_{\mathbf{p}}}p^i p^j\sigma_{ij}\,. \tag{92}$$

First we consider the case where the relaxation time grows with energy

$$\tau_R(E_{\mathbf{p}}) = \text{Const}\times\frac{E_{\mathbf{p}}}{T}\qquad \delta f = -\text{Const}\times n_{\mathbf{p}}\frac{p^i p^j}{2T^2}\sigma_{ij} \tag{93}$$

The form of this correction is known as the quadratic ansatz and was used by all hydrodynamic simulations so far[72,73,74,78]. Substituting this form into Eq. (80) one determines that for a classical gas of arbitrary mass the constant is

$$\text{Const} = \frac{\eta}{e+\mathcal{P}}\,,\qquad \text{with}\qquad \tau_R(E_{\mathbf{p}})\propto E_{\mathbf{p}}\,. \tag{94}$$

For a Bose or Fermi gas we have the replacement $n_{\mathbf{p}}\to n_p(1\pm n_p)$, and Eq. (94) is approximate holding at the few percent level. For a mixture of different classical particles with one *common* relaxation time Eq. (94) also holds. In practical simulations this correction is written covariantly and the phenomenological field $\pi^{\mu\nu} = -\eta\sigma_{\mu\nu}$ is used, leading to the final result

$$\delta f = \frac{1}{2(e+\mathcal{P})T^2}P^\mu P^\nu\pi_{\mu\nu}\,. \tag{95}$$

The quadratic ansatz may seem arbitrary, but it is often a good model of collisional energy loss and weak scattering. For instance an analysis of the leading-log Boltzmann equation (along the lines of Eq. (88)) shows that the quadratic ansatz describes the full results to 10-15% accuracy [118]. However, this agreement is in part an artifact of the leading-log, or soft scattering, approxmiation. For example, in the

leading-log plamsa the energy loss of a "high" p_T quark from the bath is given by [6]

$$\frac{dp}{dt} = \left(N_c + \frac{N_f}{2}\right) \frac{C_F g^4 T^2}{24\pi} \log\left(T/m_D\right) . \tag{96}$$

From this formula we see that the energy loss is constant at high momentum and therefore the relaxation time scales as $\tau_R \propto p$ in agreement with Eq. (93). In reality Eq. (96) is decidely wrong at large momentum where radiative energy loss becomes increasingly significant and can shorten the relaxation time. Indeed when collinear radiation is included in the Boltzman equation the quadratic ansatz becomes increasingly poor [120]. In Section 6 we will consider a relaxation time which is independent of energy as an extreme alternative

$$\tau_R \propto \text{Const} , \tag{97}$$

and explore the phenomenological consequences of this ansatz.

As discussed in Section 6, the differential elliptic flow $v_2(p_T)$ is sensitive to the form of these corrections, while the integrated v_2 is constained by the underlying hydrodynamic variables, and is largely independent of these details. This last remark should be regarded with caution as it has not been fully quantified.

6. Viscous Hydrodynamic Models of Heavy Ion Collisions

At this point we are in a position to discuss several viscous hydro models which have been used to confront the elliptic flow data. To initiate discussion, we show simulation results for $v_2(p_T)$ from Luzum and Romatschke in Fig. 12. Comparing the simulation to the "non-flow corrected" data for $p_T \lesssim 1.5\,\text{GeV}$, we can estimate an allowed range for the shear viscosity, $\eta/s \approx 0.08 \leftrightarrow 0.16$. Below we will place this conclusion in context by culling figures from related works.

A generic implementation of viscous hydrodynamics consists of several parts:

(1) At an intial time τ_o the energy density and flow velocities are specified. For Glauber initial conditions, one takes for example

$$e(\tau_o, \mathbf{x}_\perp) \propto \frac{\mathrm{d}N_{\text{coll}}}{\mathrm{d}x\,\mathrm{d}y} , \tag{98}$$

where the overall constant is adjusted to reproduce the multiplicity. The simulations assume Bjorken boost invariance and zero initial transverse velocity

$$u^\mu(\tau_o, \mathbf{x}_\perp) = (u^\tau, u^x, u^y, u^\eta) = (1, 0, 0, 0) . \tag{99}$$

The strains are taken from the Navier stokes theory for example

$$\pi^{\mu\nu}(\tau_o, \mathbf{x}_\perp) = \text{diag}\left(\pi^{\tau\tau}, \pi^{xx}, \pi^{yy}, \tau^2\pi^{\eta\eta}\right) = \left(0,\ \frac{2}{3}\frac{\eta}{\tau},\ \frac{2}{3}\frac{\eta}{\tau},\ -\frac{4}{3}\frac{\eta}{\tau}\right) , \tag{100}$$

and reflect the traceless character of shear stress.

(2) The equations of motion are solved. Viscosity modifies the energy and momentum and the associated thermodynamic conjugates T and u^μ. The viscosity

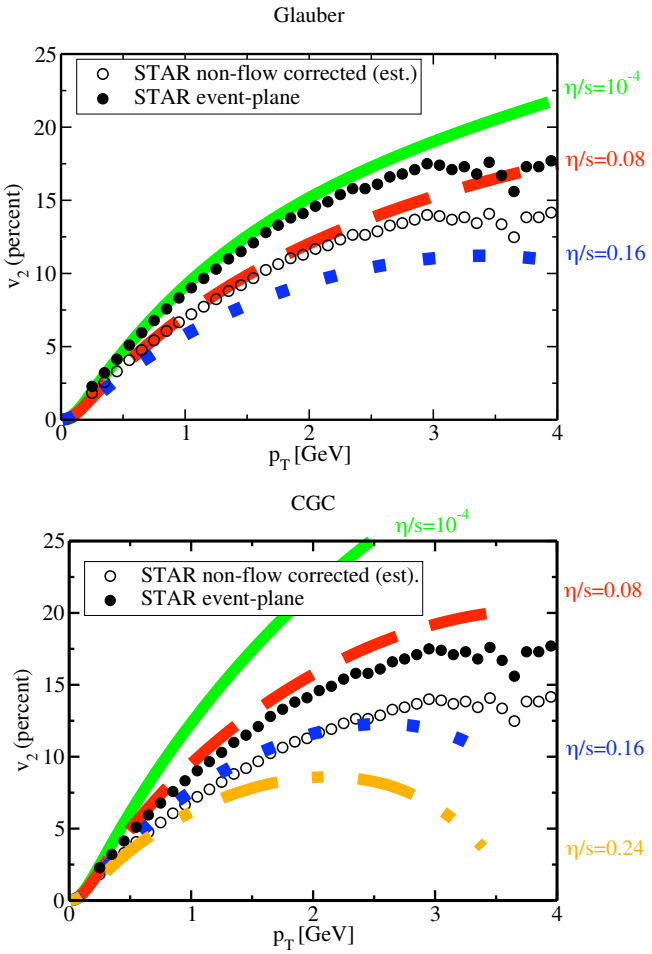

Fig. 12. Figure from Ref.[74] which shows how elliptic flow depends on shear viscosity. The theory curves are most dependable for $p_T \lesssim 1.5\,\mathrm{GeV}$ and should be compared to the "non-flow corrected" data.

also modifies off diagional components of the stress tensor through the viscous corrections $\pi^{\mu\nu}$.

(3) A freezeout condition is specified either by specifying a freezeout temperature or a kinetic condition. During the time evolution a freezeout surface is constructed. For instance the freezeout surface in Fig. 12 is the space-time three volume Σ where $T \simeq 150\,\mathrm{MeV}$.

(4) Finally, in order to compare to the data, particle spectra are computed by matching the hydrodynamic theory onto kinetic theory. Specifically final particle spectra are computed using Eq. (111). This procedure is similar to running hydro up to a particular propper time τ_f and demanding that the spectrum of

particles at that moment is the measured particle spectrum.

There are many issues associated with each of these items. The next subsections will discuss them one by one.

6.1. *Initial Conditions*

First we note that the hydrodynamic fields are initialized at a time $\tau_0 \simeq 1\,\mathrm{fm/c}$, which is arbitrary to a certain extent. Fortunately, both in kinetic theory and hydrodynamics the final results are not particularly sensitive this value [44,74]. Also, all of the current simulations have assumed Bjoken boost inariance. While this assumption should be relaxed, past experience with ideal hydrodynamics shows that the mid-rapidity elliptic flow is not substantially modified [51]. Above we have discussed one possible initialization of the hydro which makes the energy density proportional to the number of binary collisions, *e.g.* the Glauber curves of Fig. 12. Another reasonable option is to make the entropy proportional to the number of participants [73]

$$s(\tau_0, \mathbf{x}_\perp) \propto \frac{\mathrm{d}N_p}{\mathrm{d}x\mathrm{d}y}\,. \tag{101}$$

As a limit one can take the CGC model discussed in Section 2. Finally it is generally assumed that the intial transverse flow is zero

$$u_x(\tau_0, \mathbf{x}_\perp) = u_y(\tau_0, \mathbf{x}_\perp) = 0\,. \tag{102}$$

This assumption should probably lifted in future calculations and a more reasonable (but still small) estimate is given in Ref.[45].

Examining Fig. 12 and Fig. 6 we see see that there is a significant and predictable linear dependence on the eccentricity. When extracting the shear viscosity from the data, this uncertainty in the eccentricity leads to a factor of two uncertainty in the final results for the the shear viscosity. As emphasized in Section 2, the CGC model should be thought of as an upper limit to the anisotropy that can be produced in the initial state. Therefore, the uncertainty in η/s is probably not as large as dispersion in the curves would indicate. In ideal hydrodynamics, the spread in $v_2(p_T)$ resulting from the different initializations specified by Eq. (101) and Eq. (98) was studied[46], and is small compared to the difference between the Glauber and CGC curves in Fig. 12.

Once the intial conditions for the temperature and flow velocities are specified, the off diagonal components of the stress tensor $\pi^{\mu\nu}$ are determined by spatial gradients in these quantities. To second order this is given by Eq. (63) and there is no ambiguity in this result. Time derivatives may be replaced with spatial derivatives using lower order equations of motion to second order accuracy. In the phenomenological theory $\pi^{\mu\nu}$ is promoted to a dynamical variable. Clearly the appropriate initial condition for this variable is something which deviates from $-\eta\sigma^{\mu\nu}$ by second order terms. However, the extreme choice $\pi^{\mu\nu} = 0$ was studied to estimate

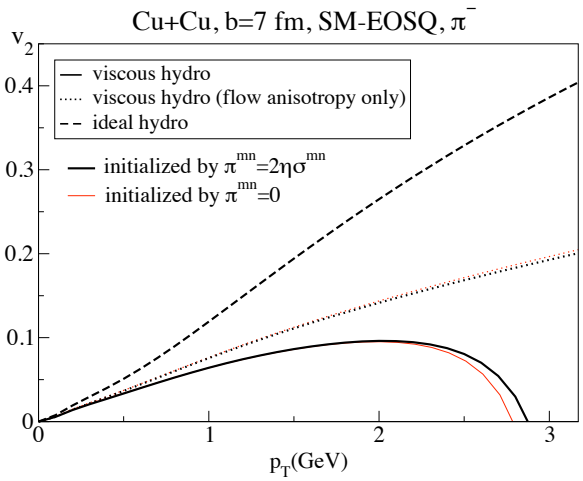

Fig. 13. Figure from Ref.[79] studying the independence of the final results on the initialization of $\pi^{\mu\nu}$.

how initial non-euilbrium effects could alter the final results. This is just an estimate since the relaxation of these fields far from equilibrium is not well captured by hydrodynamics. Nevertheless, even with this extreme choice, the stress tensor relaxes to the expected form $\pi^{\mu\nu} = -\eta\sigma^{\mu\nu}$ relatively quickly. The result is that $v_2(p_T)$ is insenstive to the different initializations of $\pi^{\mu\nu}$. This can be seen clearly from Fig. 13.

6.2. *Corrections to the Flow*

Once the initial conditions are specified, the equations of motion can be solved. First we adress the size of the viscous corrections to the temperature and flow velocities. The magnitude of the viscous corrections depends on the size of the system and the shear viscosity. Fig. 14 shows a typical result for the AuAu system. As seen from the figure the effect of viscosity on the temperature and flow velocities is relatively small.

An explanation for this result is the following[105]: In the first moments of the collision the system is expanding in the longitudinal direction and the pressure in the longitudinal directions is reduced

$$\tau^2 T^{\eta\eta} = p - \frac{4}{3}\frac{\eta}{\tau}\,. \tag{103}$$

At first sight, this means that the system cools more slowly and indeed this is initially true. However, since the shear tensor is traceles there is an increase in the transverse pressure which is uniform in all directions

$$T^{xx} = T^{yy} = p + \frac{2}{3}\frac{\eta}{\tau}\,, \tag{104}$$

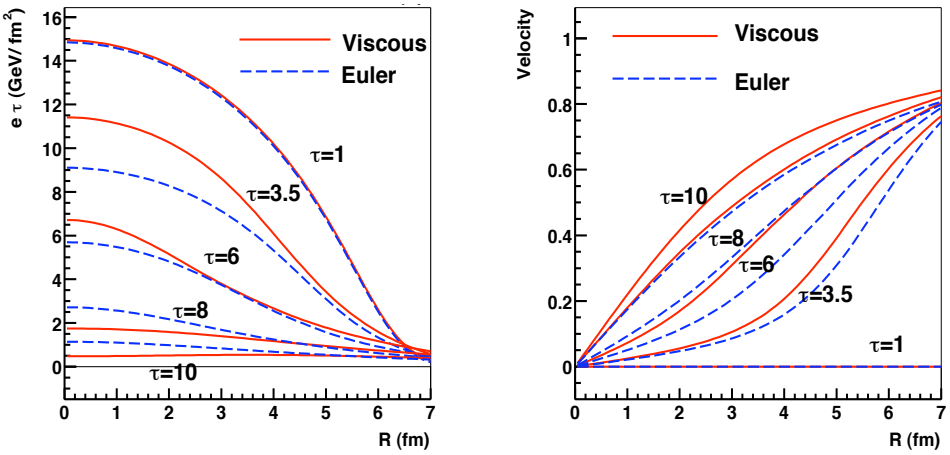

Fig. 14. A central AuAu simulation with an ideal gas equation of state $p = e/3$ and $\eta/s = 0.2$ which compares the viscous and Euler evolution[105]. The left figure shows the energy density ($\times\tau$) for different times. The right figure shows the velocity for different times.

and which ultimately increases the radial flow. Since the radial flow is larger in the viscous case, the system ultimately cools faster.

Having discussed the dependence of T and u^μ, we turn to a quantity which largely dictates the of the final elliptic flow – the momentum anisotropy [106]. The momentum anisotropy is defined as[d]

$$e_p' = \frac{\langle T^{xx} - T^{yy} \rangle}{\langle T^{xx} + T^{yy} \rangle} = \frac{\int d^2\mathbf{x}_\perp \, (T^{xx} - T^{yy})}{\int d^2\mathbf{x}_\perp \, (T^{xx} + T^{yy})} \,, \tag{105}$$

Fig. 15 illustrates how this momentum anisotropy icreases as a function of time in the CuCu and AuAu systems. Although the flow fields $T(\mathbf{x}, \tau)$ and $u^\mu(\mathbf{x}, \tau)$ are quite similar between the ideal and viscous cases, the ideal anisotropy is significantly reduced by viscous effects. The reason for this reduction is becuase the viscous stress tensor anisotropy, involves the difference

$$\Pi^{xx} - \Pi^{yy} \,,$$

in addition to the temperature and flow velocities. This additional term is ultimately responsible for the deviation of e_p' between the ideal and viscous hydrodynamic calculations. At later times there is some modification of e_p', due to the flow itself, but this is dependent on freezeout. The deviation $\Delta\Pi = \Pi^{xx} - \Pi^{yy}$ will have important phenomenological consequences in determining the viscous correction to the elliptic flow spectrum.

[d]Note there is a misprint in the original definition of ϵ_p' in Ref.[106]. Eq. (3.2) of that work used a double bracket notation indicating an energy density weight which should only be a single bracket as above. This double bracket definition (rather than Eq. (105)) was subsequently used in Ref.[73]

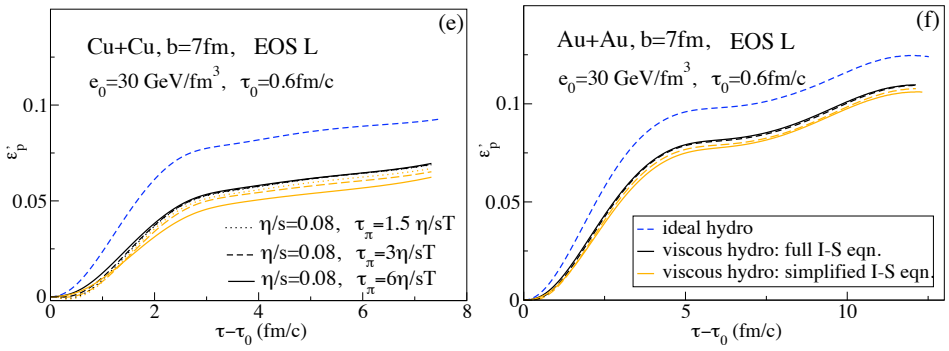

Fig. 15. Figure from Ref.[78] comparing the development of the flow anistropy e'_p (Eq. (105)) in viscous hydrodynamics relative to the ideal hydrodyanmics. The lower band of curves are all representative of viscous hydro and differ only in how the second order corrections are implemented. The anisotropy differs from ideal hydro because the anistropy involves the viscous differece, $\Pi^{xx} - \Pi^{yy}$.

6.3. *Convergence of The Gradient Expansion*

Fig. 15 also compares the simplified Israel-Stewart equation Eq. (68) to the full Israel-Stewart equation Eq. (69) as a function of the relaxation time parameter τ_π. The result supports much of the discussion given in Section 4.6. In the roughest approximation neither the simplified Israel-Stewart equation nor the full Israel-Stewart equation depend on the relaxation time parameter τ_π. When an ideal gas equation of state is used the dependence on τ_π is stronger especially for the simplified Israel-Stewart equation [78]. Note also that the dependence on τ_π is stronger in the smaller CuCu system than AuAu. However, in the conformally invariant full Israel-Stewart equation the dependence on τ_π is neglible, indicating that the result is quite close to the first order Navier Stokes theory. The more rapid convergence of the gradient expansion of the conformally invariant fluids is a result of the fact that the derivatives in the conformal case come together as

$$\tau_\pi \left[\langle D\pi^{\mu\nu} \rangle + \frac{4}{3}\pi^{\mu\nu}\nabla \cdot u \right] .$$

We have selected one figure out of many [78,73,74]. The result of the analysis is that the flow fields and $v_2(p_T)$ are largely independent of the details of the second order terms at least for $\eta/s \lesssim 0.3$. For this range of parameters hydrodynamics at RHIC is an internally consistent theory.

which is why the associated curve differs from other recent works [74,78].

6.4. *The Edge and Freeezeout*

Clearly viscous hydrodynamics is an approximation which is not valid at early times and near the edge of the nucleus. This failure afflicts the current viscous calculations at a practical level right at the moment of initialization. For instance, the longitudinal pressure

$$\tau^2 T^{\eta\eta} = p - \frac{4}{3}\frac{\eta}{\tau_0}\,, \tag{106}$$

eventually becomes negative near the edge of the nucleus indicating the need to transition to a kinetic description[7]. (Note that $p \propto T^4$ while $\eta \propto T^3$, so at sufficiently low temperatures the viscous term is always dominant regardless of the magnitude of η/s.) The current calculations simply limit the size of this correction through the phenomenological Israel-Stewart model. For example, one approach would be to take

$$\tau^2 T^{\eta\eta} = p - \tau^2 \Pi^{\eta\eta}\,, \tag{107}$$

with

$$\tau^2 \Pi^{\eta\eta} = \begin{cases} -\frac{4}{3}\frac{\eta}{\tau_o} & \text{while } 4/3\eta/\tau_0 < 0.9p \\ 0.9\,p & \text{otherwise} \end{cases}\,. \tag{108}$$

This adhoc fix is clearly not nice and points to the larger problem of freezeout which is difficult to adress with hydrodynamics itsself.

Freezeout is the colloquial term for the transition from a hydrodynamic to a kinetic regime and is impossible to separate cleanly from the viscosity itsself in a realistic nucleus-nucleus collision. Clearly as the shear viscosity is made smaller and smaller, a larger and larger space time volume is described by hydrodynamics. To estimate the size of the relevant space time region we remark that hydrodynamics is valid when the relaxation time τ_R is much smaller than the inverse expansion rate, $\tau_R \partial_\mu u^\mu \ll 1$. Therefore, in the simulations one can estimate the region of validity by monitoring the expansion rate relative the relaxation time [109,110]. Specifically, freezeout is signaled when

$$\frac{\eta}{\mathcal{P}}\partial_\mu u^\mu \sim \frac{1}{2}\,. \tag{109}$$

This combination of parameters can be motivated from the kinetic theory estimates [111]. The pressure is $\mathcal{P} \sim e\left\langle v_{\rm th}^2\right\rangle$, with $\left\langle v_{\rm th}^2\right\rangle$ the typical quasi-particle velocity. The viscosity is of order $\eta \sim e\left\langle v_{\rm th}^2\right\rangle \tau_R$ with τ_R the relaxation time. Thus hydrodyanmics breaks down when

$$\frac{\eta}{\mathcal{P}}\partial_\mu u^\mu \sim \tau_R \partial_\mu u^\mu \sim \frac{1}{2}\,. \tag{110}$$

Fig. 16 estimates the space-time region described by viscous hydrodynamics. Examining this figure we see that the time duration of the hydrodynamic regime is a relatively strong function of η/s at least for a conformal gas. In reality the

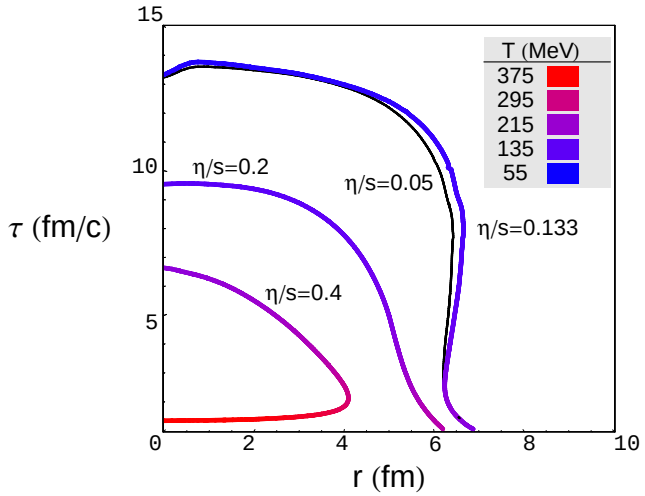

Fig. 16. This figure estimates for a conformal gas with equation of state $p = e/3$ and constant η/s the space time region described by viscous hydrodynamics [73]. The contours are where $(\eta/p)\,\partial_\mu u^\mu = 0.6$ for different values of η/s. For the smallest value $\eta/s = 0.05$ the system freezes out at a time of order $\sim 40\,\mathrm{fm}$. This unrealistically long time reflects the conformal nature of the gas as discussed in Section 4.5. For comparison we have shown the $(\eta/p)\,\partial_\mu u^\mu = 0.225$ contour for $\eta/s = 0.05$.

behaviour of the shear viscosity near the transition region will control when the hydrodynamics will end.

Clearly the surface to volume ratio in Fig. 16 is not very small. Hydrodynamics is a terrible approximation near the edge. There is a need for a model which smoothly transitions from the hydrodynamic regime in the center to a kinetic or free streaming regime at the edge. Near the phase transition kinetic theory may not be a good model for QCD, but it has the virtue that it gracefully implements this hydro to kinetic transition. Although the interactions and the quasi-particle picture of kinetic theory may be decidedly incorrect, this is unimportant in the hydrodynamic regime. In the hydrodynamic regime the only properties that determine the evolution of the system are the equation of state, $\mathcal{P}(\epsilon)$, and the shear viscosity and bulk viscosities, $\eta(\epsilon)$ and $\zeta(\epsilon)$. In the sense that they provide a reasonable guess as to how the surface to volume ratio influences the forward evolution, kinetic models can be used to estimate the shear viscosity and the estimate may be more reliable than the hydrodynamic models. A priori one should demand that the kinetic models have the same eqation of state and the same shear viscosity as expected from QCD, $\eta \propto T^3$. For instance in a kinetic model of massless particles with a constant cross section σ_o (such as studied in Ref.[57,68,69]) the shear viscosity scales as $\eta \propto T/\sigma_o$. This

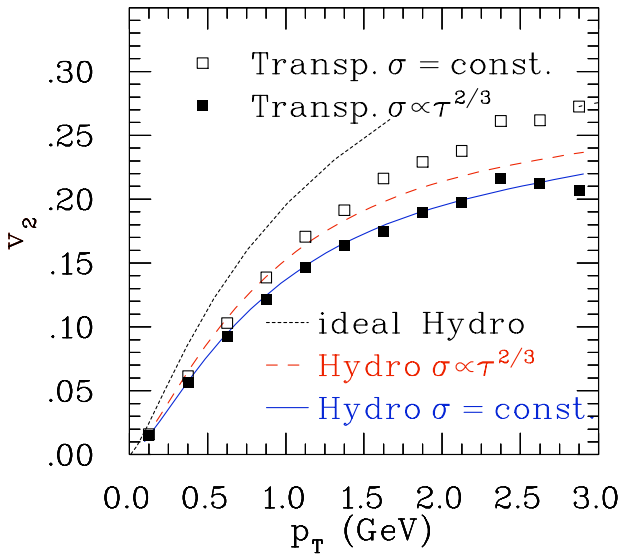

Fig. 17. Fig from Ref.[70].

difference with QCD should be born in mind when extracting conclusions about the heavy ion reaction. Further many transport models conserve particle number which is an additional conservation law not inherent to QCD; this also changes the dynamics. Keeping these reservations in mind we examine Fig. 17. This figure shows a promising comparison between kinetic theory with contant cross section (σ_o = Const) and a viscous hydrodynamic calculation with $\eta \propto T/\sigma_o$. The case with $\sigma \propto \tau^{2/3}$ will not be discussed in this review but is an attempt to mimic a fluid which has $\eta \propto T^3$ [70]

What is excititing about this figure is the fact that the hydrodynamic conclusions are largely supported by the results of a similar kinetic theory. This gives considerable confidence that the surface to volume effects are small enough that the hydrodynamc conclusions presented in Fig. 12 are largely unchanged by particles escaping from the central region. More formally the opacity is large enough to support hydrodynamics.

There have been other kinetic calculations which are working towards extraciting η/s from the heavy ion data [2,1,19]. In particular Refs.[20,21,23,24] uses a kinetic theory implementation of $2 \to 2$ and $2 \to 3$ interactions motivated by weak coupling QCD[19]. It also chooses calculates the Debye scale self consistently, *i.e.* in equlibrium one sets $m_D^2 \propto g^2 T^2$ and T changes with time. Out of equilbrium this mass scale m_D is determined from the momentum distribution of particles. Consequently this model respects the symmetry properties of high temperature QCD, i.e. the model has $\eta \propto T^3$ and does not conserve particle number. For the model

parameter $\alpha_s = 0.3 \leftrightarrow 0.5$ (which is only schematically related to the running coupling) the shear to entropy ratio is $\eta/s = 0.16 \leftrightarrow 0.08$ [24,23]. The model (known as BAMPS) is conformal and never freezes out as discussed in Section 4.5. The current implementation of BAMPS simply stops the kinetic evolution when the energy density reaches a critical value, $e_c \simeq 0.6 \leftrightarrow 1.0\,\mathrm{GeV/fm}^3$. This parameter is an abrupt way to introduce a needed scale into the problem and schematically approximates the rapid variation of the shear viscosity in this energy density range. Fig. 18 shows the time development of elliptic flow in this model and which can reproduce the observed flow only for $\eta/s = 0.16 \leftrightarrow 0.08$, depending on the model parameter e_c. The time development of v_2 seen in Fig. 18 shows that it is very difficult to separate precisely the shear viscosity in the initial stage from the freezeout process.

Clearly the transition from a hydrodynamic regime to a kinetic regime is important to clarify in the future. In the meantime most hydrodynamic groups have invoked an ad-hoc freezeout perscription. In Refs.[72,74,78,79] the hydrodynamic codes were run until a typical freezeout temperature $T_{\mathrm{fo}} \simeq 150\,\mathrm{MeV}$. Technically the freezeout surface is construced the temperature is constant is constructed by marching forward in time and triangulating the space-time surface with constant temperature In Ref.[70] a surface of constant density particle density was chosen $n \simeq 0.365/\mathrm{fm}^3$ and in Ref.[73] the surface chosen was motivated by the kinetic kinetic condition Eq. (109) given above. Ideally in the future this could be impoved by dynamically coupling the hydrodynamic evolution to a kinetic description or by simulating the entire event with a kinetic theory which closely realizes the equation of state and transport coefficients used in the hydrodynamic simlations.

6.5. *Particle Spectra*

Finally we turn to the particle spectra in viscous hydrodynamics. Ideally the system would evolve through the approximate phase transition down to sufficiently low temperatures where the dynamics could be described either with viscous hydrodynamics or with the kinetic theory of a Hadron Resonance Gas (HRG). In reality this does not seem particularly likely since the system is already expanding three dimensionally and the scales are approximately fixed (see Section 4.5). The estimates of the shear viscosity to entropy ratio in a hadronic gas are reliable for $T \lesssim 130\,\mathrm{MeV}$ and do not support this optimistic picture (see Section 3). In seems quite unlikely that there is equilibrium evolution in the HRG below a temperature of $T \simeq 150\,\mathrm{MeV}$. Clearly the dynamics is extremely complex during the quark-hadron transition which takes in place for an energy density of $e \simeq 0.5 \leftrightarrow 1.2\,\mathrm{GeV/fm}^3$. In this range the temperature changes by only $\Delta T \simeq 20\,\mathrm{MeV}$. However, the hydrodynamic simulations evolve this complicated region for a significant time period, $\tau \simeq 4\,\mathrm{fm} \leftrightarrow 7\,\mathrm{fm}$. This transition region can be seen in the AuAu plots in Fig. 15.

The pragmatic approach to this complexity is to compute the quasi-particle spectrum of hadrons at a temperature of $T \simeq 150\,\mathrm{MeV}$. Since the HRG describes the QCD thermodyanmics well, this pragmatism is fairly well motivated. The ap-

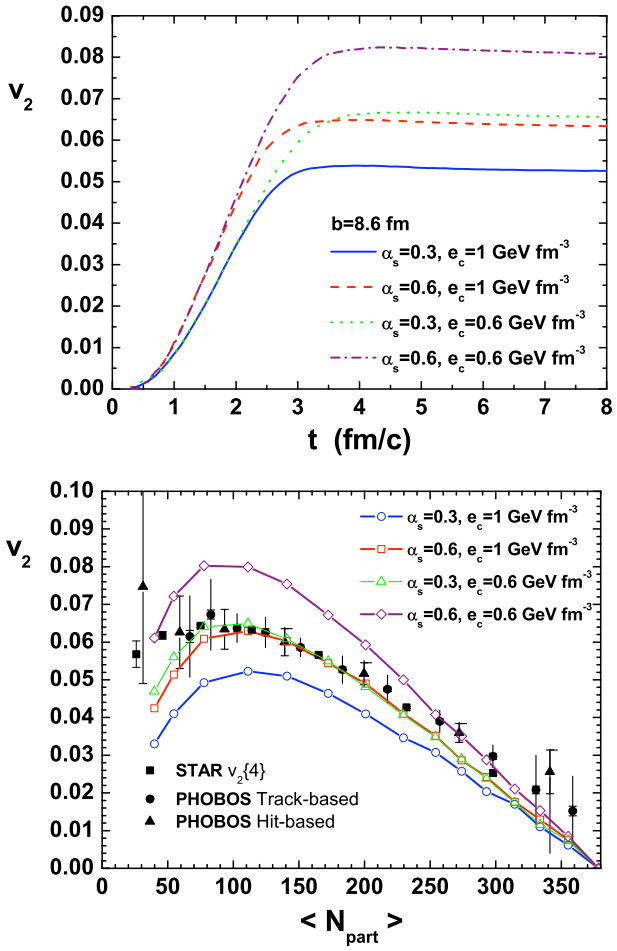

Fig. 18. (Top) The development of elliptic flow v_2 as a function of time in the BAMPS model[20]. (Bottom) The final elliptic flow as a function of centrality. The shear viscosity to entropy ratio η/s corresponding to the model parameter $\alpha_s = 0.3 \leftrightarrow 0.6$ was estimated in Ref.[24,23] and is $\eta/s = 0.16 \leftrightarrow 0.08$. The evolution is stopped with the energy density reaches a critical value of e_c.

proach conserves energy and momentum and when viscous corrections are included also matches the strains across the transition. In ideal hydrodynamics simulations the subsequent evolution of the hadrons has been followed with hadronic cascade models [55,52,51]. The result of these hybrid models is that the hadronic rescattering is essentially unimportant for the $v_2(p_T)$ observables presented here.

Technically, the procedure is the following: along the freezeout surface the spec-

trum of particles is computed with the Cooper-Frye formula

$$E\frac{dN^a}{d^3\mathbf{p}} = \frac{g_a}{(2\pi)^3}\int_\Sigma \mathrm{d}\Sigma_\mu P^\mu\, f^a(-P\cdot u/T)\,, \tag{111}$$

where a labels the particle species,

$$f^a(-P\cdot u) = n^a(-P\cdot u/T) + \delta f^a(-P\cdot u/T)\,, \tag{112}$$

is the distribution function (see Section 5), and g_a the spin-isospin degeneracy factor for each particle included. In practice, the Boltzman approximation is often sufficient. In Ref.[74] all particles where included up to mass of $m_{\rm res} < 2.0\,\mathrm{GeV}$ and then subsequently decayed. In other works a simple gas was used to study various aspects of viscous hydrodynamics divorced from this complex reality[73,70].

All of the viscous models used the quadratic ansatz discussed in Section 5, writing the change to the distribution function of the a-th particle type as

$$f^a \to n^a + \delta f^a\,, \tag{113}$$

with δf^a given by

$$\delta f^a = \frac{1}{2(e+\mathcal{P})T^2} n^a(1\pm n^a) P^\mu P^\nu \pi_{\mu\nu}\,. \tag{114}$$

In the simple gas models there was only one particle type[73,70]. In Refs.[72,79] the constant was taken to be the same for all particle species.

Before continuing we review the elements that go into a complete hydrodynamic calculation. First initial conditions are specified (see Section 6.1.) Then the equations are solved with the viscous term (see Section 6.2.) After this a freezeout surface is specified (see Section 6.4 for the limitations of this.) Finally we compute spectra which using Eq. (111) and Eq. (114). This particle spectra can ultimately be compared to the observed elliptic flow. With this oversight we take a more nuanced look at Fig. 12.

To isolate the viscous modifications due to the flow and the viscous modifications due to the distribution function, we turn to Fig. 19. Examining this figure we see that a significant part of the corrections due to the shear viscosity are from the distribution function rather than the flow. Although the magnitude of the flow modifications depends on the details of freezeout, this dependence on δf is the typical and somewhat distressing result. We emphasize however that it is inconsistent to drop the modifications due to δf. The result of dropping the δf means that the energy and momentum of the local fluid cell $T^{\mu\nu}u_\nu$ is matched by the particle content, but the off diagonal strains $\pi^{\mu\nu}$ are not reproduced. The assumption underlying the comparison of viscous hydrodynamics to data is that the form of these off diagonal strains is largely unmodified from the Navier Stokes limit during the freezeout process. As the particles are "freezing out" this is a reasonable assumption. However, since these strains are only partially constrained by conservation laws, this assumption needs to tested against kinetic codes as already emphasized

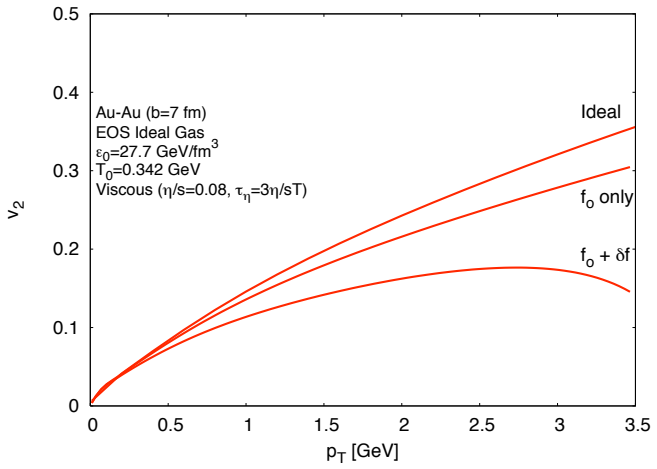

Fig. 19. $v_2(p_T)$ from Ref.[73] showing the dependence on the flow f_o and the dependence on the viscous modification of the distribution function δf. The result depends to a certain extent on freezeout.

above. This freezeout problem is clearly an obstacle to a reliable extraction of η/s from the data.

Although the dependence on δf in $v_2(p_T)$ is undesirable, the viscous modifications of *itegrated* elliptic flow v_2 largely reflects the modifications to the stress tensor itself. The observation is that the stress anistropy e'_p (see Eq. (105)) determines the average flow according to a simple rule of thumb[106]

$$v_2 \simeq \frac{1}{2} e'_p \,. \tag{115}$$

Fig. 20 shows e'_p and v_2 as a function of centrality. The figure supports this rule and suggests that sufficiently integrated predictions from hydrodynamics do not depend on the detailed form of the viscous distrbution.

To corroborate this conclusion we turn to an analysis originally presented by Ollitrault[107] and subsequently generalized to the viscous case[73,18]. First we parametrize the single particle spectrum dN/dp_T with an an exponential and $v_2(p_T)$ as linearly rising, *i.e.*

$$\frac{1}{p_T}\frac{dN}{dp_T} \simeq C e^{-p_T/T} \,, \qquad \text{and} \qquad v_2 \propto p_T \,. \tag{116}$$

With this form one finds quite generally that the p_T^2 weighted elliptic flow is twice the average v_2

$$2v_2 \simeq A_2 \equiv \frac{\langle p_x^2 - p_y^2 \rangle}{\langle p_x^2 + p_y^2 \rangle} \,. \tag{117}$$

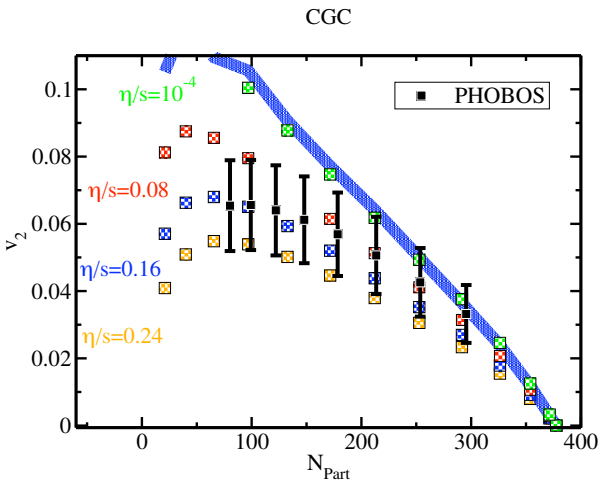

Fig. 20. Dependence of elliptic flow versus some centrality from Ref.[74]. The lines show the results of viscous hydrodynamics and corresponding points show the anistropy of the stress tensor $0.5\, e'_p$ (see Eq. (105)) for different values of η/s. The sensitivity to the quadratic ansatz is estimated in the text and corresponds to half the difference between the red and blue curves. The huerstic rule $v_2 \simeq 0.5\, e'_p$ is motivated in the text.

The p_T^2 weighted elliptic flow has a much closer relationship to the underlying hydrodynamic variables. Indeed we will show how this simple rule of thumb arises and that it is largely independent of the details of δf.

To this end we evaluate the sphericity tensor which will have a simple relationship to A_2

$$S^{\mu\nu\rho} = S_I^{\mu\nu\rho} + S_V^{\mu\nu\rho} = \int \frac{d^3\mathbf{p}}{(2\pi)^3 E_{\mathbf{p}}} P^\mu P^\nu P^\rho \left[n(-P\cdot u) + \delta f(-P\cdot u) \right] \qquad (118)$$

Then using the Cooper-Frye formula (with $d\Sigma_\mu = (\tau d^2\mathbf{x}_\perp, 0, 0, 0)$) the assymetry at any given moment in time is

$$A_2 = \frac{\int d^2\mathbf{x}_\perp \left(S^{0xx} - S^{0yy} \right)}{\int d^2\mathbf{x}_\perp \left(S^{0xx} + S^{0yy} \right)} \,. \qquad (119)$$

The sphericity tensor consists of an ideal piece and a viscous piece

$$f \to n + \delta f \,, \qquad S^{\mu\nu\rho} \to S_I^{\mu\nu\rho} + S_V^{\mu\nu\rho} \,. \qquad (120)$$

First we consider the ideal piece and work in a classical massless gas approximation for ultimate simplicity. The tensor is a third rank symmetric tensor and can be decomposed as

$$S_I^{\mu\nu\rho} = A(T) u^\mu u^\nu u^\rho + B(T) \left(u^\mu g^{\nu\rho} + \text{perms} \right) \,. \qquad (121)$$

Here $A(T)$ and $B(T)$ are thermodyanmic functions and are given n by

$$\frac{A}{6} = B = \int \frac{d^3\mathbf{p}}{(2\pi)^3}\frac{p^2}{3} n_{\mathbf{p}} = (e+p)T\,. \tag{122}$$

For Bose and Fermi gasses this relation is approximate. Thus the ideal piece of the sphericity tensor is largely constrained by thermodynamic functions. The viscous piece is largely constrained by the shear viscosity. As discussed in Section 5 we parametrize the δf with $\chi(p)$

$$\delta f = -n_{\mathbf{p}}\,\frac{\chi(p)}{(P\cdot U)^2} P^\mu P^\nu \sigma_{\mu\nu}\,. \tag{123}$$

While the precise form of the viscous correction $\chi(p)$ depends on the details of the microscopic interactions, it is constrained by the shear viscosity

$$\eta = \frac{2}{15}\int \frac{d^3\mathbf{p}}{(2\pi)^3} p\,\chi(p) n_{\mathbf{p}}\,. \tag{124}$$

Substituting the viscous parametrization into the definition of the sphericity we find

$$S^{0xx} = -C(T)\left[u^0\sigma^{xx} + 2u^x\sigma^{x0}\right]\,, \tag{125}$$

$$\simeq -C(T) u^0\sigma^{xx}\,, \tag{126}$$

where $C(T)$ is

$$C(T) = \frac{2}{15}\int \frac{d^3\mathbf{p}}{(2\pi)^3} p^2\chi(p) n_{\mathbf{p}}\,. \tag{127}$$

For simplicity we have assumed that the flow is somewhat non-relativistic so that $u^x\pi^{x0}$ is $O(v^2)$ compared to $u^0\pi^{xx}$. To get a feeling for how sensitive the results are to the quadratic ansatz we will work with a definite functional form

$$\chi(p) = \text{Const}\times p^{2-\alpha}\,. \tag{128}$$

In a relaxation time approximation discussed in Section 5, $\alpha = 0$ corresponds to a relaxation time which increases with p_T while $\alpha = 1$ corresponds to a relaxation time indepent of p_T. Substituting this ansatz we find

$$C(T) \simeq (6-\alpha)T\eta \qquad 0<\alpha<1\,, \tag{129}$$

Having assembled the ingredients we can write down an approximate formula for A_2

$$A_2 \simeq \frac{\int \mathrm{d}^2\mathbf{x}_\perp\, Tu^0\left[(e+p)(u_xu_x - u_yu_y) + (1-\frac{\alpha}{6})\,(\pi^{xx}-\pi^{yy})\right]}{\int \mathrm{d}^2\mathbf{x}_\perp\, Tu^0\left[(e+p)(u_xu_x + u_yu_y) + (e+p)/3 + (1-\frac{\alpha}{6})\,(\pi^{xx}+\pi^{yy})\right]}\,, \tag{130}$$

with $0<\alpha<1$. This is the desired formula which expresses the observed elliptic flow in terms of the hydrodynamic variables. To reiterate the coefficient α changes the functional form the viscous distribtuion function and $0<\alpha<1$ is a reasonable

range; $\alpha = 0$ is the usual quadratic ansatz. It might be useful to compare this to the formula to the definition of ϵ'_p

$$e'_p = \frac{\int \mathrm{d}^2\mathbf{x}_\perp \ [(e+p)(u_x u_x - u_y u_y) + (\pi^{xx} - \pi^{yy})]}{\int \mathrm{d}^2\mathbf{x}_\perp \ [(e+p)(u_x u_x + u_y u_y) + 2p + (\pi^{xx} + \pi^{yy})]} \,. \tag{131}$$

Thus while e'_p is not exactly equal to the A_2 of Eq. (130), it is close enough to explain the hueristic rule, $2v_2 \simeq e'_p$.

The overall symmetries and dimensions of the sphericity tensor suggests a definition for an analgous quantity in hydrodynamics

$$S^{\mu\nu\rho}_{\rm hydro} = T\left[(e+p)u^\mu u^\nu u^\rho + \frac{1}{6}(e+p)(u^\mu g^{\nu\rho} + \text{perms}) + (u^\mu \pi^{\nu\rho} + \text{perms})\right] . \tag{132}$$

In fact in a classical massless gas approxmation with the quadratic ansatz, the analysis sketched above shows that

$$S^{\mu\nu\rho}_{\rm hydro} = \frac{1}{6} S^{\mu\nu\rho} \,. \tag{133}$$

The important point for this review is that from Eq. (130) we see that the *integrated* elliptic flow is relatively insensitive to the quadratic form for the viscous distribution function. More specifically the uncertainty is $\sim 15\%$ of $A_2^{\rm ideal} - A_2^{\rm viscous}$, *i.e.* about half the difference between the blue and red curves in Fig. 20. The quadratic ansatz (which has been used by all hydrodynamic simulations) can be a poor approximation when collinear emission processes are included in the Boltzman description[17].

Clearly adressing more completely the uncertainties associated with the particle content and microscopic interactions in Fig. 20 is a task for the future. Nevertheless, it does seem that sufficiently integrated quantities will reflect rather directly the bulk properties of the hydrodynamic motion in a way that can be quantified.

7. Summary and Outlook

Acknowledgements

We gratefully acknowledge discussions Raimond Snellings, Kevin Dusling, Paul Romatschke, Peter Petreczky. D.T. is supported by the U.S. Department of Energy under an OJI grant DE-FG02-08ER41540 and as a Sloan Fellow.

8. Appendices

References

1. V. Greco, M. Colonna, M. Di Toro and G. Ferini, arXiv:0811.3170 [hep-ph].
2. G. Ferini, M. Colonna, M. Di Toro and V. Greco, Phys. Lett. B **670**, 325 (2009) [arXiv:0805.4814 [nucl-th]].
3. P. Huovinen and P. V. Ruuskanen, Ann. Rev. Nucl. Part. Sci. **56**, 163 (2006) [arXiv:nucl-th/0605008].
4. The data presented are from the thesis Dr. Yuting Bai.

5. see for example, B. I. Abelev *et al.* [STAR Collaboration], Phys. Rev. C **77**, 054901 (2008) [arXiv:0801.3466 [nucl-ex]].
6. E. Braaten and M. H. Thoma, Phys. Rev. D **44**, 2625 (1991). Phys. Rev. D **44**, 1298 (1991).
7. M. Martinez and M. Strickland, arXiv:0902.3834 [hep-ph].
8. M. A. York and G. D. Moore, arXiv:0811.0729 [hep-ph].
9. B. Betz, D. Henkel and D. H. Rischke, arXiv:0812.1440 [nucl-th].
10. see for example, T. Schaefer and D. Teaney, arXiv:0904.3107 [hep-ph].
11. G. Aarts, C. Allton, J. Foley, S. Hands and S. Kim, Phys. Rev. Lett. **99**, 022002 (2007) [arXiv:hep-lat/0703008].
12. H. B. Meyer, arXiv:0809.5202 [hep-lat].
13. P. F. Kolb and U. W. Heinz, arXiv:nucl-th/0305084.
14. K. Itakura, O. Morimatsu and H. Otomo, Phys. Rev. D **77**, 014014 (2008) [arXiv:0711.1034 [hep-ph]].
15. see for example, A. Milov [PHENIX Collaboration], J. Phys. Conf. Ser. **5**, 17 (2005) [arXiv:nucl-ex/0409023].
16. G. D. Moore and O. Saremi, JHEP **0809**, 015 (2008) [arXiv:0805.4201 [hep-ph]].
17. Guy Moore, private communication.
18. D. Teaney, and K. Dusling, in progress.
19. Z. Xu and C. Greiner, Phys. Rev. C **71**, 064901 (2005) [arXiv:hep-ph/0406278].
20. Z. Xu and C. Greiner, Phys. Rev. C **79**, 014904 (2009) [arXiv:0811.2940 [hep-ph]].
21. Z. Xu, C. Greiner and H. Stocker, Phys. Rev. Lett. **101**, 082302 (2008) [arXiv:0711.0961 [nucl-th]].
22. I. Bouras *et al.*, arXiv:0902.1927 [hep-ph].
23. A. El, A. Muronga, Z. Xu and C. Greiner, arXiv:0812.2762 [hep-ph].
24. Z. Xu and C. Greiner, Phys. Rev. Lett. **100**, 172301 (2008) [arXiv:0710.5719 [nucl-th]].
25. See for example, M. Le Bellac, *Thermal Field Theory* (Cambridge University Press, Cambridge, England, 1996).
26. N. Demir and S. A. Bass, arXiv:0812.2422 [nucl-th].
27. A. Bazavov *et al.*, arXiv:0903.4379 [hep-lat].
28. R. Baier, A. H. Mueller, D. Schiff and D. T. Son, Phys. Lett. B **502**, 51 (2001) [arXiv:hep-ph/0009237].
29. P. Aurenche, F. Gelis, R. Kobes and H. Zaraket, Phys. Rev. D **58**, 085003 (1998) [arXiv:hep-ph/9804224].
30. E. Beth and G. E. Uhlenbeck, Physica **4**, 915 (1937).
31. R. Venugopalan and M. Prakahsh, Nucl. Phys. A. **546**, 718 (1992). ‘
32. M. L. Miller, K. Reygers, S. J. Sanders and P. Steinberg, Ann. Rev. Nucl. Part. Sci. **57**, 205 (2007) [arXiv:nucl-ex/0701025].
33. J. Y. Ollitrault, A. M. Poskanzer and S. A. Voloshin, arXiv:0904.2315 [nucl-ex].
34. M. Miller and R. Snellings, “Eccentricity fluctuations and its possible effect on elliptic flow arXiv:nucl-ex/0312008.
35. S. A. Voloshin, A. M. Poskanzer, A. Tang and G. Wang, Phys. Lett. B **659**, 537 (2008) [arXiv:0708.0800 [nucl-th]].
36. R. S. Bhalerao and J. Y. Ollitrault, Phys. Lett. B **641**, 260 (2006) [arXiv:nucl-th/0607009].
37. B. Alver *et al.*, Phys. Rev. C **77**, 014906 (2008) [arXiv:0711.3724 [nucl-ex]].
38. S. A. Voloshin, A. M. Poskanzer and R. Snellings, arXiv:0809.2949 [nucl-ex].
39. B. Alver *et al.* [PHOBOS Collaboration], “System size, energy, pseudorapidity, and centrality dependence of elliptic Phys. Rev. Lett. **98**, 242302 (2007) [arXiv:nucl-ex/0610037].

40. D. Kharzeev, E. Levin and M. Nardi, Nucl. Phys. A **730**, 448 (2004) [Erratum-ibid. A **743**, 329 (2004)] [arXiv:hep-ph/0212316].
41. H. J. Drescher, A. Dumitru, A. Hayashigaki and Y. Nara, "The eccentricity in heavy-ion collisions from color glass condensate Phys. Rev. C **74**, 044905 (2006) [arXiv:nucl-th/0605012].
42. H. J. Drescher, A. Dumitru and J. Y. Ollitrault, arXiv:0706.1707 [nucl-th]; in N. Armesto *et al.*, "Heavy Ion Collisions at the LHC - Last Call for Predictions," J. Phys. G **35**, 054001 (2008).
43. T. Lappi and R. Venugopalan, Phys. Rev. C **74**, 054905 (2006) [arXiv:nucl-th/0609021].
44. D. Molnar, private communication.
45. J. Vredevoogd and S. Pratt, arXiv:0810.4325 [nucl-th].
46. P. F. Kolb, U. W. Heinz, P. Huovinen, K. J. Eskola and K. Tuominen, Nucl. Phys. A **696**, 197 (2001) [arXiv:hep-ph/0103234].
47. M. Grmela, H.C. Öttinger, Phys. Rev. E **56**, 6620 (1997). H.C. Öttinger, M. Grmela, Phys. Rev. E **56**, 6633 (1997). H.C. Öttinger, Phys. Rev. E **57**, 1416 (1993).
48. J. Adams *et al.* [STAR Collaboration], Nucl. Phys. A **757**, 102 (2005) [arXiv:nucl-ex/0501009].
49. K. Adcox *et al.* [PHENIX Collaboration], Nucl. Phys. A **757**, 184 (2005) [arXiv:nucl-ex/0410003].
50. T. Hirano, private communication.
51. T. Hirano and Y. Nara, Nucl. Phys. A **743**, 305 (2004) [arXiv:nucl-th/0404039].
52. D. Teaney, J. Lauret and E. V. Shuryak, arXiv:nucl-th/0110037. *ibid*, Phys. Rev. Lett. **86**, 4783 (2001)
53. P. F. Kolb, P. Huovinen, U. W. Heinz and H. Heiselberg, Phys. Lett. B **500**, 232 (2001) [arXiv:hep-ph/0012137].
54. P. Huovinen, P. F. Kolb, U. W. Heinz, P. V. Ruuskanen and S. A. Voloshin, Phys. Lett. B **503**, 58 (2001) [arXiv:hep-ph/0101136].
55. C. Nonaka and S. A. Bass, Phys. Rev. C **75**, 014902 (2007)
56. P. Danielewicz and M. Gyulassy, Phys. Rev. D **31**, 53 (1985).
57. H. J. Drescher, A. Dumitru, C. Gombeaud and J. Y. Ollitrault, Phys. Rev. C **76**, 024905 (2007) [arXiv:0704.3553 [nucl-th]].
58. M. Asakawa, T. Hatsuda and Y. Nakahara, Prog. Part. Nucl. Phys. **46**, 459 (2001) [arXiv:hep-lat/0011040].
59. F. Karsch, E. Laermann, P. Petreczky, S. Stickan and I. Wetzorke, Phys. Lett. B **530**, 147 (2002) [arXiv:hep-lat/0110208].
60. P. Petreczky and D. Teaney, Phys. Rev. D **73**, 014508 (2006) [arXiv:hep-ph/0507318].
61. G. Aarts and J. M. Martinez Resco, JHEP **0204**, 053 (2002) [arXiv:hep-ph/0203177].
62. H. B. Meyer, arXiv:0704.1801 [hep-lat].
63. P. Arnold, G. D. Moore and L. G. Yaffe, JHEP **0305**, 051 (2003) [arXiv:hep-ph/0302165].
64. G. Baym, H. Monien, C. J. Pethick and D. G. Ravenhall, Phys. Rev. Lett. **64** (1990) 1867.
65. G. Policastro, D. T. Son and A. O. Starinets, Phys. Rev. Lett. **87**, 081601 (2001) [arXiv:hep-th/0104066].
66. P. Kovtun, D. T. Son and A. O. Starinets Phys. Rev. Lett. **94**, 111601 (2005 [arXiv:hep-th/0405231]
67. D. Molnar and M. Gyulassy, Nucl. Phys. A **697**, 495 (2002) [Erratum-ibid. A **703**, 893 (2002)] [arXiv:nucl-th/0104073].
68. C. Gombeaud and J. Y. Ollitrault, Phys. Rev. C **77**, 054904 (2008) [arXiv:nucl-

th/0702075].
69. P. Huovinen and D. Molnar, Phys. Rev. C **79**, 014906 (2009) [arXiv:0808.0953 [nucl-th]].
70. D. Molnar and P. Huovinen, J. Phys. G **35**, 104125 (2008) [arXiv:0806.1367 [nucl-th]].
71. D. Teaney, Phys. Rev. C **68**, 034913 (2003) [arXiv:nucl-th/0301099].
72. P. Romatschke and U. Romatschke, Phys. Rev. Lett. **99**, 172301 (2007) [arXiv:0706.1522 [nucl-th]].
73. K. Dusling and D. Teaney, Phys. Rev. C **77**, 034905 (2008) [arXiv:0710.5932 [nucl-th]].
74. M. Luzum and P. Romatschke, Phys. Rev. C **78**, 034915 (2008) [arXiv:0804.4015 [nucl-th]].
75. R. Baier, P. Romatschke, D. T. Son, A. O. Starinets and M. A. Stephanov, JHEP **0804**, 100 (2008) [arXiv:0712.2451 [hep-th]].
76. S. Bhattacharyya, V. E. Hubeny, S. Minwalla and M. Rangamani, JHEP **0802**, 045 (2008) [arXiv:0712.2456 [hep-th]].
77. M. Natsuume and T. Okamura, Phys. Rev. D **77**, 066014 (2008) [Erratum-ibid. D **78**, 089902 (2008)] [arXiv:0712.2916 [hep-th]].
78. H. Song and U. W. Heinz, Phys. Rev. C **78**, 024902 (2008) [arXiv:0805.1756 [nucl-th]].
79. H. Song and U. W. Heinz, Phys. Rev. C **77**, 064901 (2008) [arXiv:0712.3715 [nucl-th]].
80. For a recent account see, D. Kharzeev, E. Levin and M. Nardi, arXiv:0707.0811 [hep-ph].
81. J. D. Bjorken, Phys. Rev. D **27**, 140 (1983).
82. G. Baym, Phys. Lett. B **138** (1984) 18.
83. M. Gyulassy, Y. Pang and B. Zhang, Nucl. Phys. A **626**, 999 (1997) [arXiv:nucl-th/9709025].
84. L. D. Landau and E. M. Lifshitz, *Fluid Mechanics* (Pergamon Press, London, 1959).
85. I. Müller, Z. Phys. **198**, 329 (1967).
86. W. Hiscock, L. Lindblom, Phys. Rev. **D31**, 725 (1985).
87. W. A. Hiscock and L. Lindblom, Annals Phys. **151**, 466 (1983).
88. W. A. Hiscock and L. Lindblom, Phys. Rev. D **35**, 3723 (1987).
89. W. Israel, Ann. Phys. **100** (1976) 310
90. W. Israel and J. M. Stewart, Annals Phys. **118**, 341 (1979).
91. R. Geroch and L. Lindblom, Phys. Rev. D **41**, 1855 (1990).
92. D. Pavón, D. Jou and J. Casas-Vásquez, Ann. Inst. Henri Poincaré, Sect. A **36**, 79 (1982).
93. H. C. Öttinger, Physica A **254** (1998) 433-450.
94. R. Geroch and L. Lindblom, Annals. Phys. **207**, 394 (19901.
95. Lee Lindblom, arXiv:gr-qc:9508058.
96. D. Forster, *Hydrodynamics, Fluctuations, Broken Symmetry, and Correlation Functions*, Perseus Books (1990).
97. D. Teaney, Phys. Rev. D **74**, 045025 (2006) [arXiv:hep-ph/0602044].
98. Azwinndini Muronga Phys. Rev. C **69** 034903, (2004); Phys. Rev. C **76**, 014909 (2007).
99. A. Muronga and D. H. Rischke, arXiv:nucl-th/0407114.
100. M. Prakash, M. Prakash, R. Venugopalan and G. Welke, Phys. Rept. **227**, 321 (1993); see also R. Venugopalan, Ph.D. thesis, Stony Brook (1992).
101. P. Arnold, C. Dogan and G. D. Moore, Phys. Rev. D **74**, 085021 (2006) [arXiv:hep-ph/0608012].
102. K. Huebner, F. Karsch and C. Pica, Phys. Rev. D **78**, 094501 (2008) [arXiv:0808.1127 [hep-lat]].
103. In the transition region there could be corrections to this statement do to the

physics of scale breaking see, D. Kharzeev and K. Tuchin, JHEP **0809**, 093 (2008) [arXiv:0705.4280 [hep-ph]].
104. L. Pareschi, SIAM J. Number. Anal **39** (2001). pp. 1395-1417.
105. Derek Teaney, J. Phys. G **30** S1247-S1250 (2004).
106. P. F. Kolb, J. Sollfrank, and U. Heinz, Phys. Rev. C **65**, 054909 (2000).
107. Jean-Yves Ollitrault, Phys. Rev. D **46**, 229-245 (1992).
108. Jean-Yves Ollitrault, private communication.
109. U. W. Heinz, K. S. Lee and M. J. Rhoades-Brown, Phys. Rev. Lett. **58**, 2292 (1987).
110. C. M. Hung and E. V. Shuryak, Phys. Rev. C **57**, 1891 (1998) [arXiv:hep-ph/9709264].
111. F. Reif, "Fundamentals of Statistical Physics", McGraw-Hill (1965)
112. F. Cooper and G. Frye, Phys. Rev. D. **10**, 186 (1974).
113. T. Hirano, U. W. Heinz, D. Kharzeev, R. Lacey and Y. Nara, Phys. Lett. B **636**, 299 (2006) [arXiv:nucl-th/0511046].
114. L. P. Kadanoff and P. C. Martin, Ann. Phys. **24**, 419 (1963).
115. Derek Teaney, Phys. Rev. D **74**, 045025 (2006).
116. P. Petreczky and D. Teaney, Phys. Rev. D **73**, 014508 (2006).
117. C. Adler . *et. al.,* STAR Collaboration, Phys. Rev. C **66**, 034904 (2002).
118. Peter Arnold, Guy D. Moore, and Laurence G. Yaffe, J. High Energy Phys. **11**, 001 (2000).
119.
120. Guy D. Moore, private communication.